Comparative chemical kinetic analysis and skeletal mechanism generation for syngas combustion with NO_x chemistry

Quan-De Wang[1,2,*], Yanjin Sun[2], Henry J. Curran[2,*]

[1] Low Carbon Energy Institute and School of Chemical Engineering, Jiangsu Province Engineering Laboratory of High Efficient Energy Storage Technology and Equipments, China University of Mining and Technology, Xuzhou, 221008, People's Republic of China

[2] Combustion Chemistry Centre, School of Chemistry, Ryan Institute, MaREI, National University of Ireland Galway, University Road, Galway, H91 TK33, Ireland

*Corresponding author. E-mail address: quandewang@cumt.edu.cn (Q.-D. Wang); henry.curran@nuigalway.ie (H. J. Curran)

Abstract

Emission of nitrogen oxides (NO_x) are one of the major environmental concerns arising from the combustion of syngas. Strategies to reduce emission and improve the efficiency of syngas combustion can be developed using computational fluid dynamic simulations to design cleaner and more efficient combustors. Toward this end, an accurate and efficient chemical kinetic mechanism that can describe the combustion chemistry of syngas with NO_x under engine-relevant conditions is critical. In this work, a comprehensive survey of detailed mechanisms available in the literature for syngas/NO_x combustion reaction system is first conducted. A systematic and comparative chemical kinetic analysis of five detailed mechanisms is performed based on reaction pathway and sensitivity analyses to identify the key reactions of the nitrogen species for a wide range of mixtures including the formation of NO_x during syngas combustion, ignition of NH_3, H_2/N_2O, and H_2/NO_2 mixtures. Comparisons of the reaction pathways from different detailed mechanisms indicate that the detailed

chemistry is controlled by a small set of reactions and species. Recent high-level theoretical studies on HONO and HNO_2 chemistry including previously neglected important reactions are updated. The rate constants for $HNO + O_2 = NO + H\dot{O}_2$ are calculated using *ab initio* calculations in this work. An efficient high-fidelity skeletal mechanism consisting of 27 species and 130 reactions is developed based on a combination of the directed relation graph with error propagation (DRGEP) method and the simplified iterative screening and structure analysis (ISSA) method. Compared to the detailed mechanisms, the skeletal mechanism retains the major species and reactions for the syngas/NO_x system and is validated against typical experimental data resulting in a very good performance.

Keywords: Combustion; syngas; NO_x chemistry; mechanism reduction; chemical kinetics

1. Introduction

Combustion has been the major process of power generation and will continue to dominate into the future. As the world's energy demands and environmental concerns continue to increase, novel ideas and innovations in the areas of fuels and combustors to reduce emission and improve efficiency are needed to achieve cleaner and more efficient combustion. Syngas, composed of varying amounts of hydrogen (H_2) and carbon monoxide (CO), is expected to be a potential alternative fuel for energy generation because it can be largely derived from biomass/coal gasification and can significantly improve combustion efficiency in stationary gas turbines via Integrated Gasification Combined Cycle (IGCC) systems.[1-3] Compared to conventional fuels such as coal for power generation, one of the major advantages for syngas is the lack of particle matter (PM) emissions and corrosive ash elements. However, due to increasingly stringent emission regulations, the emission of nitrogen oxides (NO_x) as the major drawback has become a major challenge for syngas combustion. As available

computational power continues to grow, computational fluid dynamic (CFD) simulations have become an important tool in the design of advanced combustion systems with low-NO_x emissions and improved efficiency. It is now generally recognized that these CFD simulations must necessarily incorporate realistic descriptions of the chemical kinetics of fuel combustion and NO_x formation.[4, 5] Hence, a large body of work has been dedicated to improve the chemistry of syngas and nitrogen chemistry in combustion.

The development of detailed chemical kinetic mechanisms for syngas is essential to understand not only the combustion properties of H_2 and CO themselves, but also the larger hierarchical hydrocarbon systems which rely on this core chemistry. A large number of detailed reaction mechanisms for syngas combustion with a focus on hydrogen combustion have been developed and continue to be updated, see e.g., Ó Conaire *et al.*,[6] Konnov,[7, 8] Hong *et al.*,[9] and Kéromnès *et al.*[10] These detailed reaction mechanisms were mainly validated through selected experimental targets and were not extensively validated at high pressures and temperatures relevant to practical combustor conditions. The detailed mechanism developed by Kéromnès *et al.*[10] for syngas combustion was validated against the most extensive experimental targets for H_2 and syngas. According to a systematic comparison of error function values in the prediction of H_2 combustion by Varga *et al.*,[11] the Kéromnès mechanism exhibits the best performance covering a wide range of experimental targets compared with 13 published mechanisms, and thus is selected as the base mechanism for syngas in this work.

The nitrogen chemistry in combustion has been extensively studied after Miller and Bowman[12] published their review thirty years ago. Detailed chemical kinetic mechanisms to describe the NO_x formation process during combustion of hydrocarbon and oxygenated fuels with focus on small

$H_2/C_1–C_2$ hydrocarbons have been proposed by different research groups.[13-18] A most recent study by Glarborg *et al.*[19] comprehensively revisited this topic and they also proposed a detailed reaction mechanism with updated thermochemistry and reaction rate constants from recent advances in experiments and high-level theoretical calculations. Generally, reaction mechanisms for syngas combustion with NO_x chemistry are usually defined as sub-mechanisms in these detailed chemical kinetic models except some proposed mechanisms specifically for NO_x formation during syngas combustion. For example, Zhang *et al.*[20] recently developed a detailed mechanism to describe the pyrolysis and oxidation of the H_2/NO_x and syngas/NO_x systems by using the Kéromnès mechanism[10] for syngas. These detailed kinetic mechanisms developed by different research groups exhibit different performances in predicting combustion properties.

The underlying reason for the different predictabilities of combustion properties using different detailed mechanisms is caused by the different species and reaction paths embodied in them, including their corresponding thermochemistry and reaction rates. Hence, not only evaluating the comparative mechanism performances, but also carrying out detailed comparisons of the reaction lists, reaction rates and thermochemistry of different mechanisms is helpful in refining them. Sirumalla *et al.*[21] performed comparisons of detailed kinetic mechanisms using butanol isomers as an example and revealed significant discrepancies in the thermochemistry of many species and rates of many reactions. However, such comparisons require large computational resources since detailed combustion mechanisms of complicated fuels can contain thousands of species and reactions. Furthermore, the large size of a detailed mechanism may also limit its application in CFD simulations for engine design due to the tremendous computational resources needed. Therefore, decreasing the size of a detailed mechanism is necessary to incorporate realistic combustion chemistry with CFD simulations. Thus,

mechanism reduction has been extensively studied in the past three decades. Although a series of reduced mechanisms for H_2 and syngas were developed,[22-24] very few reduced mechanisms have been developed for syngas combustion including NO_x chemistry. In addition, the discrepancies among detailed mechanisms developed by different authors need to be clarified.

Based on the above considerations, this work aims to develop an efficient high-fidelity skeletal mechanism that is able to describe the combustion chemistry of syngas with NO_x chemistry under practical combustor conditions. To achieve this, a systematic and comparative chemical kinetic analysis of five detailed mechanisms for the syngas/NO_x system has been performed by comparing reaction pathway analyses and the associated rate constants of key reactions. An updated detailed mechanism is proposed with updated kinetics from recent high-level theoretical studies.[25-27] Finally, a skeletal mechanism consisting of 27 species and 130 reactions has been developed based on a combination of the DRGEP and ISSA methods.

This paper is organized as follows. The methodology used in this work is outlined in Section 2, including an overview of detailed mechanism for syngas combustion with NO_x chemistry and a concise explanation of the mechanism reduction and analysis methods. Section 3 describes the comprehensive comparisons of different detailed mechanisms and the skeletal mechanism reduction results. The performance and applicability of the skeletal mechanisms are further investigated for a broad range of conditions relevant to engine simulations. Section 4 lists our conclusions.

2. Methods

2.1. Mechanism overview and development

A series of detailed mechanisms describing syngas/NO_x oxidation have been developed. However, most of them have been developed based on loose combinations of different parts from a small

number of systematically developed mechanisms and validated for their target experiments. Thus, in the present work, we do not intend to provide a comprehensive model performance of all of these mechanisms. Instead, this work aims to clarify the chemical kinetics of NO_x chemistry during syngas combustion and develop an efficient skeletal mechanism describing syngas/NO_x combustion. The detailed mechanism developed by Zhang *et al.*[10] has been selected as the initial mechanism because this sub-mechanism provides the best performance and the detailed mechanism was validated against a large number of experimental data over a wide range of combustion conditions. Major reaction pathways, species and reactions related to NO_x sub-mechanism are compared with GRI-Mech 3.0[28] and three other detailed mechanisms developed by Konnov,[13] Glarborg *et al.*,[19] and Mathieu *et al.*[14] These selected mechanisms represent state-of-the-art kinetic mechanisms for NO_x chemistry in combustion, based on a systematic evaluation of the knowledge of thermochemistry and reaction rates from theoretical/experimental works.

2.2. Mechanism analysis method

To perform comparative chemical kinetic analyses and determine the reaction paths of the skeletal mechanism for the studied syngas/NO_x system, an elemental flux analysis for N is performed. Details of the analytical method can be found in references.[29, 30] In addition, brute-force sensitivity analysis is employed to identify the dominant ignition chemistry. Based on these systematic analyses, key reactions and species affecting model performances are identified and discussed in detail.

2.3. Skeletal mechanism generation

Mechanism reduction methods have been extensively studied and applied to a wide range of combustion reaction systems.[5] Skeletal reduction, aiming to remove unimportant species and

reactions for the target system, is the basis for further mechanism optimization or time-scale reduction. To obtain a minimal skeletal mechanism, skeletal reduction methods are combined together, starting by removing unimportant species, followed by removing unimportant reactions because one species generally corresponds to five reactions and the computational cost of simulations typically scales quadratically with the number of species and linearly with the number of reactions.[5] A variety of methodologies have been developed for this purpose. In this work, an integrated method that combines the DRGEP[31] and ISSA methods[32-34] has been employed. The DRGEP method is selected as the first step as this method has proven to be more efficient compared to other DRG-based methods.[35] The ISSA method is then used to remove unimportant species and reactions simultaneously as it is efficient in capturing the major reaction pathways in the mechanism reduction process compared to other pure mathematical methods.

To achieve a comprehensive high-fidelity skeletal mechanism for the syngas/NO_x combustion system, skeletal reduction is performed over a wide range of conditions. Specifically, the DRGEP and ISSA methods are successively applied to reaction state points densely sampled from constant volume ignition simulations over a wide range of simulation conditions within the parameter range of pressures from 1 to 30 atm and equivalence ratios from 0.5 – 2.0 at initial temperatures in the range 800–1700 K for $H_2/CO/O_2/N_2$, $H_2/NO_2/O_2/Ar$, $H_2/N_2O/O_2/Ar$, $H_2/NO/O_2/Ar$ and $NH_3/O_2/N_2$ mixtures. Reaction states solely sampled from ignition simulations for mechanism reduction have been confirmed to be efficient in generating skeletal mechanisms, which can also exhibit good performance in predicting other combustion properties including laminar flame speed, species concentration profiles, etc.[5, 34, 35] The species H_2, CO, N_2O, NO_2, NO, NH_3 together with H atom are selected as targeted species during the reduction processes.

3. Results and discussions

3.1. Preliminary mechanism analysis

Table 1 lists the species related to the syngas/NO_x combustion reaction system considered in the six selected detailed mechanisms and the species retained in the derived final skeletal mechanism. In fact, in developing detailed mechanisms, species and reactions are interdependent and mutual. The sub-mechanism for syngas in the detailed mechanism developed by Mathieu *et al.*[14] were based on Metcalfe *et al.*[36] and Kéromnès *et al.*,[10] and the NO_x section was largely based on the work of Dagaut *et al.*,[18] which mainly focused on the formation and oxidation of hydrogen cyanide (HCN). This sub-mechanism was also updated in the Glarborg mechanism.[19] Hence, the detailed mechanism of Dagaut *et al.*[18] is not discussed in detail. GRI-Mech 3.0[28] was published about twenty years ago representing the advanced level at that time and has been the industrial standard for the last two decades. The mechanism developed by Konnov was mainly focused on NCN pathway of prompt-NO formation. From Table 1, the Zhang mechanism contains the most comprehensive nitrogen related species for syngas combustion except for the HNNO species, which only exists in Konnov mechanism. The HNNO species is an energetic adduct for the reaction of Ḣ atom with N_2O. At low temperatures, the addition reaction to the formation of cis- and trans-HNNO isomers can be dominant due to addition-stabilization process.[37, 38] But the bimolecular channels of the reaction for Ḣ + N_2O to the formation of N_2 + ȮH, NH + ṄO, NNH + Ö become dominant at high temperatures with N_2 + ȮH being the most important.[39] The HNNO species and its related reactions were added to Zhang mechanism to test its importance in syngas/NO_x reaction system at combustion relevant conditions and nearly no influence is observed in the comparison. Table 2 compares the thermodynamic properties of selected important N-containing species, and it can be seen that the differences of the thermodynamic

properties in the selected detailed mechanisms are very small. The transport properties of the nitrogen related species in Table 1, mostly based on GRI-Mech 3.0, agree well with each other among the mechanisms, and thus model performances should be mainly controlled by the chemical kinetics.

Table 1. Species related to the syngas/NO_x combustion reaction system in the selected detailed mechanisms and the derived skeletal mechanism.

	Zhang *et al.*[20]	Skeletal mechanism (this work)	Glarborg *et al.*[19]	Konnov[13]	GRI-Mech 3.0[28]	Dagaut *et al.*[18]	Mathieu *et al.*[14]
Shared species	N NH NH_2 NH_3 NNH ṄO NO_2 N_2O HNO						
Individual species	N_2H_2	N_2H_2	N_2H_2	N_2H_2			
	N_2H_3		N_2H_3	N_2H_3			
	N_2H_4		N_2H_4	N_2H_4			
	HONO	HONO	HONO	HONO		HONO	HONO
	HNOH		HNOH	HNOH		HNOH	HNOH
	H_2NO	H_2NO	H_2NO	H_2NO		H_2NO	H_2NO
	NO_3		NO_3	NO_3		NO_3	NO_3
	HNO_2	HNO_2	HNO_2			HNO_2	HNO_2
	$HONO_2$		$HONO_2$			$HONO_2$	$HONO_2$
	HNO_3			HNO_3			
	H_2NN		H_2NN				
	HON	HON	HON			HON	HON
	NH_2OH		NH_2OH	NH_2OH			
	N_2O_4			N_2O_4			N_2O_4
	N_2O_3			N_2O_3			N_2O_3
				HNNO			

Table 2. Thermodynamic properties of selected important N-containing species in the reaction mechanisms. Units are kcal mol^{-1} for $\Delta_f\mathbf{H}^{\mathbf{0}}_{\mathbf{298}}$, and cal mol^{-1} K^{-1} for S and C_p. Temperatures are in K.

Species	**Mechanism**	$\Delta_f\mathbf{H}^{\mathbf{0}}_{\mathbf{298}}$	$\mathbf{S}^{\mathbf{0}}_{\mathbf{298}}$	$\mathbf{C}_{p,\,300\,\mathrm{K}}$	$\mathbf{C}_{p,\,400}$	$\mathbf{C}_{p,\,500}$	$\mathbf{C}_{p,\,600}$	$\mathbf{C}_{p,\,800}$	$\mathbf{C}_{p,\,1000}$	$\mathbf{C}_{p,\,1500}$
NH_3	GRI 3.0	–10.97	46.07	8.58	9.30	10.10	10.90	12.32	13.60	15.98
	Konnov	–10.98	46.07	8.58	9.28	10.10	10.90	12.30	13.54	15.84
	Glarborg	–10.89	46.07	8.53	9.24	10.04	10.81	12.22	13.44	15.76
	Zhang	–10.43	45.99	8.52	9.24	10.00	10.80	12.40	13.90	16.46
NH_2	GRI 3.0	45.90	46.60	8.14	8.36	8.66	9.00	9.74	10.48	11.94
	Konnov	45.20	46.60	8.14	8.36	8.66	8.98	9.70	10.44	11.88
	Glarborg	44.46	46.57	8.05	8.24	8.51	8.81	9.50	10.19	11.64

	Zhang	44.58	46.51	8.08	8.28	8.54	8.86	9.56	10.26	11.68
NH	GRI 3.0	85.30	43.31	7.02	7.02	7.04	7.10	7.28	7.52	8.12
	Konnov	85.33	43.31	7.02	7.02	7.04	7.10	7.28	7.52	8.12
	Glarborg	85.75	43.32	6.97	6.97	6.99	7.04	7.22	7.47	8.07
	Zhang	85.11	43.26	7.00	7.00	7.02	7.06	7.24	7.48	8.02
ṄO	GRI 3.0	21.81	50.37	7.18	7.20	7.34	7.52	7.84	8.18	8.60
	Konnov	21.81	50.37	7.18	7.20	7.34	7.52	7.84	8.18	8.60
	Glarborg	21.78	50.37	7.14	7.16	7.29	7.47	7.83	8.12	8.55
	Zhang	21.65	50.32	7.16	7.18	7.30	7.46	7.82	8.10	8.54
N_2O	GRI 3.0	19.50	52.58	9.32	10.28	11.04	11.66	12.62	13.28	14.20
	Konnov	19.50	52.58	9.32	10.28	11.04	11.66	12.62	13.28	14.20
	Glarborg	19.73	52.58	9.25	10.21	10.96	11.59	12.54	13.20	14.15
	Zhang	19.74	52.45	9.20	10.12	10.88	11.50	12.42	13.04	13.90
NO_2	GRI 3.0	8.17	57.40	8.96	9.74	10.50	11.16	12.12	12.76	13.52
	Konnov	8.17	57.40	8.96	9.74	10.50	11.16	12.12	12.76	13.52
	Glarborg	8.14	57.40	8.90	9.68	10.44	11.09	12.05	12.67	13.49
	Zhang	7.14	57.31	8.90	9.68	10.40	11.04	12.00	12.58	13.36
HNO	GRI 3.0	25.40	52.80	8.16	8.54	9.04	9.60	10.64	11.50	13.30
	Konnov	25.60	52.80	8.16	8.54	9.04	9.60	10.64	11.48	13.36
	Glarborg	25.56	52.79	8.09	8.45	8.96	9.51	10.52	11.36	13.17
	Zhang	25.82	52.71	8.12	8.48	8.96	9.52	10.56	11.40	12.82
NNH	GRI 3.0	59.63	53.65	8.34	8.86	9.44	9.98	10.86	11.56	12.56
	Konnov	59.63	53.65	8.34	8.86	9.44	9.98	10.86	11.56	12.56
	Glarborg	59.70	53.65	8.22	8.62	9.11	9.61	10.52	11.26	12.36
	Zhang	60.28	53.59	8.32	8.78	9.32	9.88	10.92	11.72	13.08

3.2. Comparative reaction path analysis

To achieve a comprehensive understanding of the chemical kinetics of the syngas/NO_x reaction system, a systematic reaction path analysis is performed for a wide range of mixtures including the formation of NO_x during syngas combustion, $NH_3/O_2/N_2$, $H_2/N_2O/O_2/Ar$, and $H_2/NO_2/O_2/Ar$ mixtures. The reaction pathways of the formation of NO species for ignition delay time (IDT) simulations of a 50/50 H_2/CO syngas mixture in air is analyzed using the five detailed mechanisms. Figure 1 shows the N element flux analysis at 20% H_2 consumption. The reaction pathways demonstrate the thermal formation of ṄO during syngas combustion. All five mechanisms reveal that the thermal formation of ṄO is mainly initiated by the reaction of N_2 with oxygen atom: $N_2 + Ö = ṄO + N$, and the N

radical subsequently reacts with O_2 and ȮH to form ṄO. However, the other reaction pathways leading to the formation of ṄO from N_2 exhibit large deviations in different mechanisms. The results based on the Zhang and Glarborg mechanisms show very similar reaction pathways because they mainly use the same reaction rate constants for the key reactions. The Konnov mechanism and GRI-Mech 3.0 predict that the NNH pathway is competitive with the N_2O pathway. At low temperature conditions, the pathway through NNH and N_2O become important.

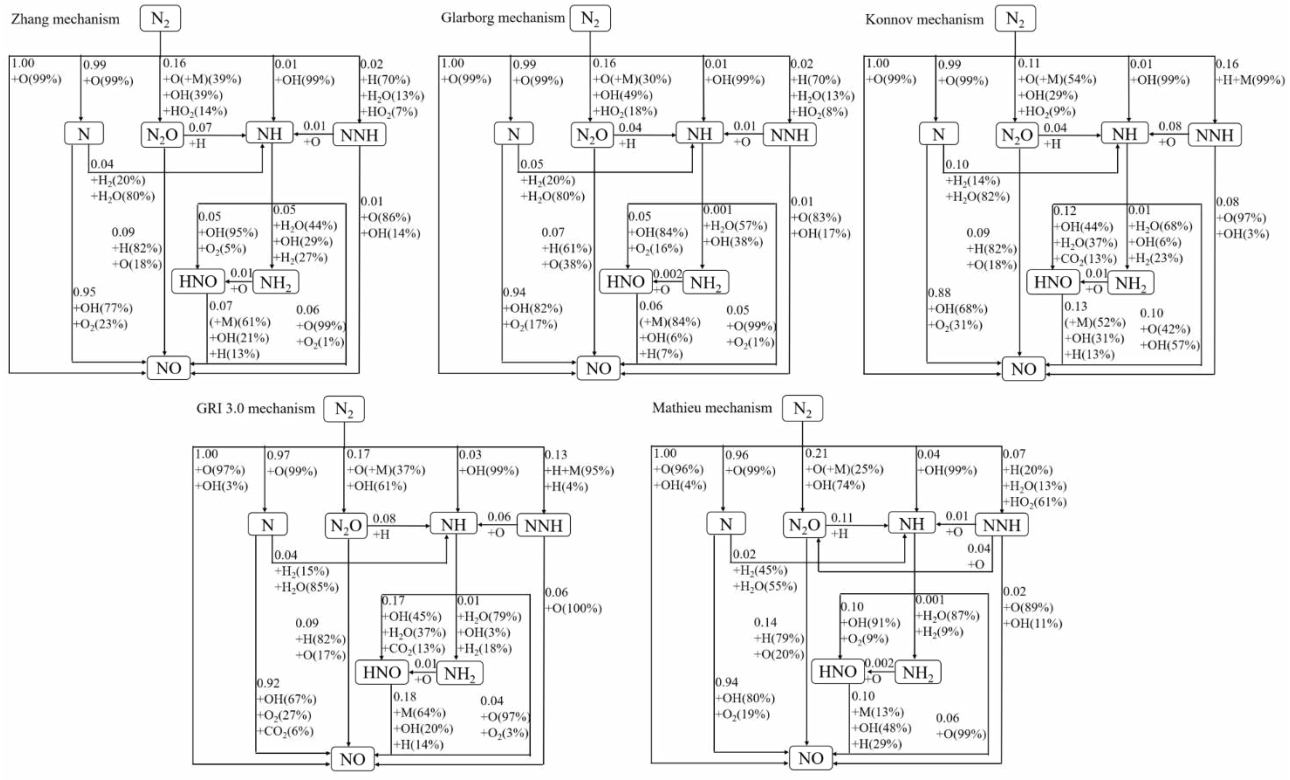

Figure 1. Element flux analysis of N during ignition delay time simulation of syngas/air mixture at initial temperature of 1200 K with equivalence ratio (φ) of 1.0 and pressure of 20 atm.

The ignition delay time of $H_2/O_2/Ar$ and $H_2/O_2/Ar$ mixtures with NO_2 and N_2O as additives[40, 41] are used to benchmark these detailed mechanisms. The major reaction path for N_2O during the ignition of the $H_2/N_2O/O_2/Ar$ mixture is simple and N_2O mainly converts into N_2. The reaction of N_2O + Ḣ producing N_2 + ȮH completely controls the transformation with the exception of $N_2O + H_2 = N_2 + H_2O$ only presents in Zhang's mechanism also contributes to the transformation of N_2O into

N_2, especially at low temperatures (< 1200 K). Figure 1 shows that at 20% H_2 consumption with an initial temperature of 900 K, the contributions of these two reactions of N_2O with Ḣ and H_2 are 1% and 99%, respectively, while the contributions of the reaction of N_2O with H_2 decreases to 6% at 1200 K. The rate constant for this reaction has a large uncertainty. Mulvihill *et al.*[42] recently recommended a new rate constant for this reaction based on shock tube studies of IDTs and H_2O time histories, which is three times lower than the rate constant used in Zhang's mechanism. For $H_2/NO_2/O_2/Ar$ mixtures, the reaction $NO_2 + Ḣ = ṄO + ȮH$ is completely dominant. Other species including HONO, HNO_2, and HNO also participate in the flux, but their relative percentages are minor.

Syngas from gasification or de-volatilization of solid fuels may also include ammonia (NH_3), which is the key volatile-N species in combustion. Although a number of modeling and experimental studies on NH_3 oxidation chemistry have been reported,[19, 43] the development of reliable detailed mechanisms for NH_3 oxidation remains challenging. Figure 2 shows the element flux analysis results for IDT simulations of NH_3/air mixture at an initial temperature of 1500 K for an equivalence ratio of 1.0 at a pressure of 20 atm. No ignition is predicted at temperatures below 1500 K using GRI-Mech 3.0. The Zhang mechanism and Glarborg mechanism exhibit very similar reaction pathways, while the Konnov and Mathieu mechanisms show very different analysis results. All of the mechanisms reveal that the initial reaction pathway for NH_3 oxidation is the formation of NH_2 through H-atom abstraction reactions by ȮH radicals, and Ḣ and Ö atoms, but the relative contributions from these reactions are different due to differing reaction rate constants. It is shown that the most important reaction path of NH_2 is through the reactions with NH_2 and NH forming N_2H_2, which are not considered in the Mathieu mechanism and in GRI-Mech 3.0. A major difference of the Konnov mechanism compared to the Zhang and Glarborg mechanisms is the direct formation of HNO through

NH_2 via reactions with Ö and O_2. Another difference is that the reactions contribute to the formation of NNH and finally to N_2. At the conditions studied, the decomposition reaction totally controls the transformation from NNH to N_2 in Konnov mechanism, and the reaction of NNH with O_2 also plays an important role. Besides these differences, it can be concluded that although the relative transformations among major species and the contributions from dominant reactions are different for the considered reactive mixtures, the key reactions and species retained in different detailed mechanisms are mostly identical and the different performances of these detailed mechanisms are essentially affected by the use of different reaction rate constants for a small number of key reactions. Besides element flux analyses of the mixtures, we also employ sensitivity analyses to identify and compare key reactions in these detailed mechanisms.

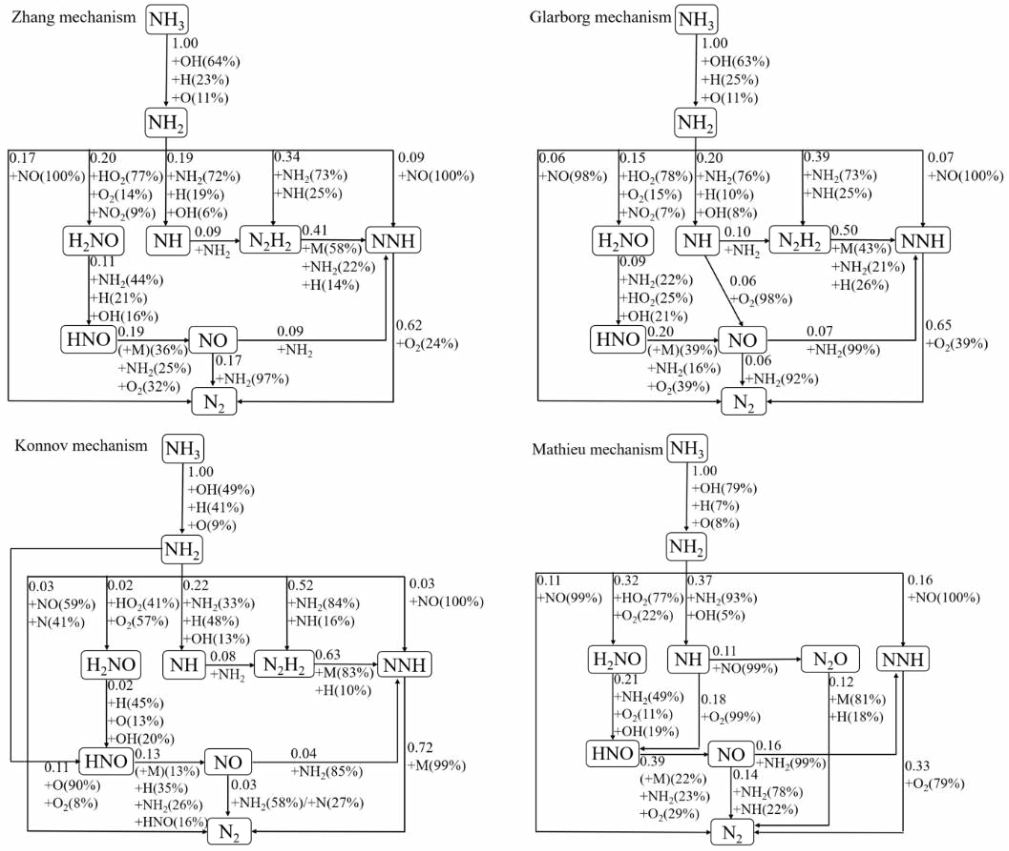

Figure 2. Element flux analysis of N during ignition delay time simulation of NH_3/air mixture at initial temperature of 1500 K with equivalence ratio (φ) of 1.0 and pressure of 20 atm.

3.3. Sensitivity analysis and mechanism updates

In an attempt to elucidate the selection of accurate rate constants for important reactions, a brute-force sensitivity analysis is employed for IDT simulations to identify important reactions and their differences in the various detailed mechanisms and to provide further help in the selection of accurate reaction rate constants. The sensitivity coefficient of the rate constants of reaction *i* on IDT is defined by the following formulation:

$$\text{Sensitivity}(i) = \frac{\tau_{ign}(2k_i) - \tau_{ign}(k_i)}{\tau_{ign}(k_i)} \quad (1)$$

where k_i is the rate constants of reaction *i*, $\tau_{ign}(2k_i)$ is the IDT when the rate of reaction *i* is doubled, and $\tau_{ign}(k_i)$ is the nominal value of the IDT. Therefore, a negative sensitivity coefficient value means that the IDT becomes shorter when the rate of reaction *i* is doubled and the overall reaction rate increases. Brute-force sensitivity analyses to IDT for H_2/N_2O/Ar and H_2/NO_2/Ar mixtures are conducted using the five detailed mechanisms at a pressure of 20 atm and at temperatures of 950 and 1500 K, Figure 3.

According to Figure 3, only four reactions, namely, N_2O (+M) = N_2 + Ö (+M), Ḣ + N_2O = NH + ṄO, Ḣ + N_2O = N_2 + ȮH and H_2 + N_2O = N_2 + H_2O have a large effect on the IDT predictions of the H_2/N_2O/Ar mixture excluding the H_2 chemistry. The sensitivity coefficients of the two reaction channels of Ḣ + N_2O are smaller compared with the other two reactions. The sensitivity coefficient for the decomposition of N_2O increases as temperature increases, while the sensitivity coefficient for the reaction H_2 + N_2O = N_2 + H_2O decreases as temperature increases. The rate constants of these two reactions both show a positive influence on the reactivity of the H_2/N_2O/Ar mixture. It is noticeable that the reaction H_2 + N_2O = N_2 + H_2O is only included in the Zhang mechanism which is the second most sensitive reaction, having a positive influence in increasing reactivity.

Zhang mechanism

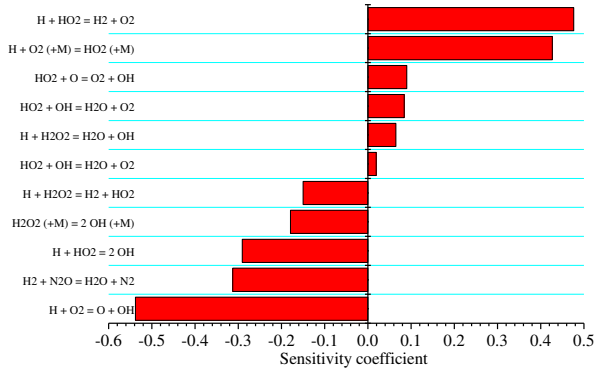

Zhang mechanism

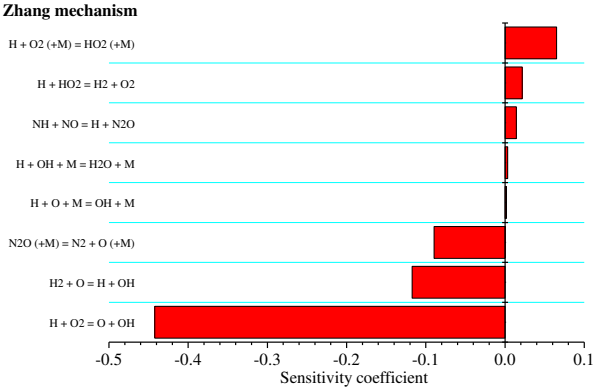

Glarborg mechanism

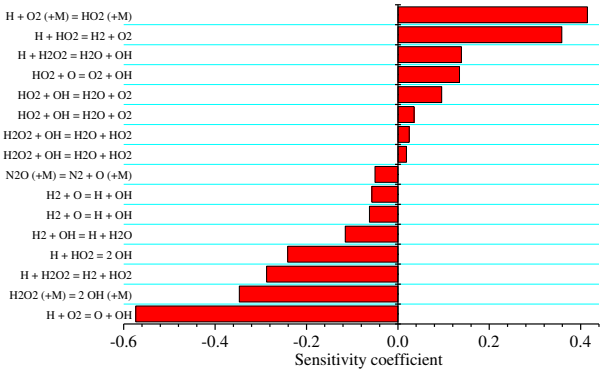

Glarborg mechanism

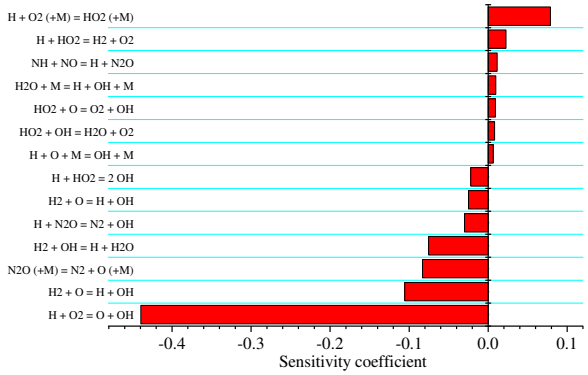

Konnov mechanism

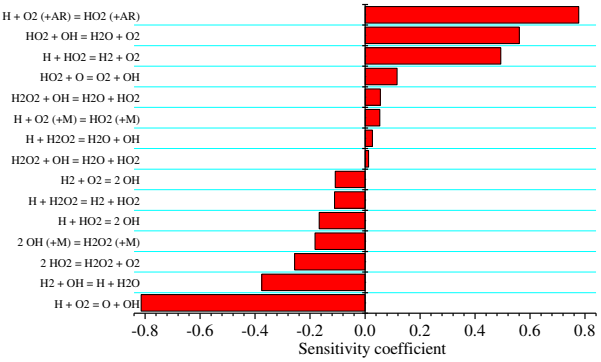

Konnov mechanism

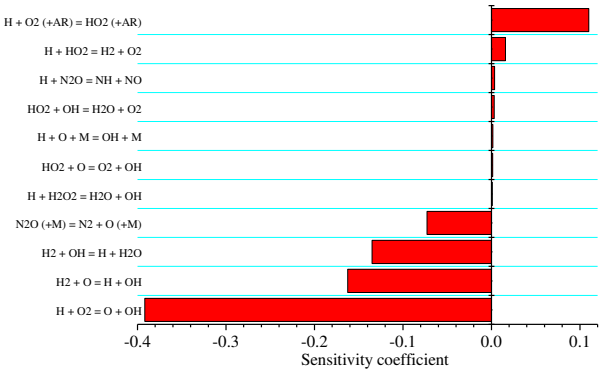

Mathieu mechanism

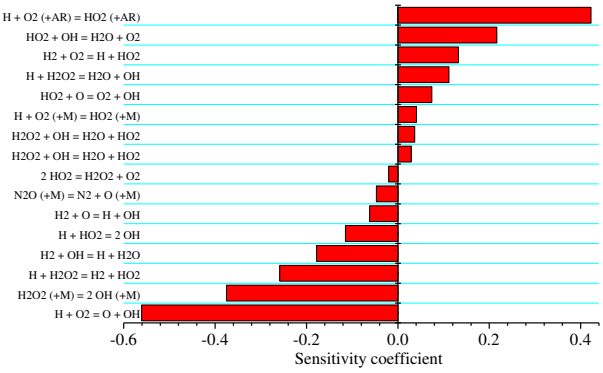

Mathieu mechanism

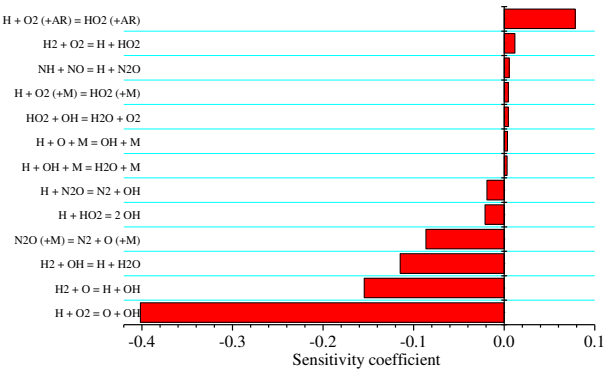

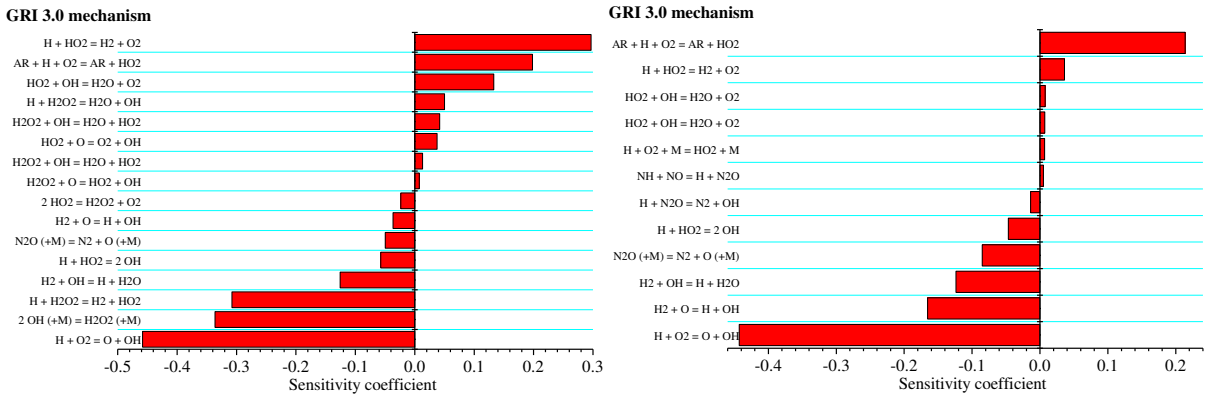

Figure 3. Sensitivity analysis of auto-ignition for H_2/N_2O/Ar mixture (0.01/0.0016/0.9784) by using the five detailed mechanisms at pressure of 20 atm and temperatures of 950 K (left) and 1500 K (right).

As for the sensitivity analysis results shown in Figure 4 for the H_2/NO_2/Ar mixture, the five mechanisms exhibit very different characteristics. (1) At 950 K, the most sensitive reactions in the Zhang and Glarborg mechanisms are identical, although the sensitivity coefficients are slightly different. The recombination reaction of ȮH and ṄO leading to the formation of HONO decreases the reactivity, while the reactions of NO_2 with H_2 / H_2O increase the reactivity on doubling their rate constants. (2) The sensitive reactions related to nitrogen species in the Konnov and Mathieu mechanisms are different. The recombination reactions of HONO show large sensitivity coefficients in the Konnov mechanism, which results from the significantly larger rate constants employed in the Konnov mechanism than those used in other mechanisms. However, this reaction exhibits very small contribution to reaction activity based on our flux analysis. (3) The reaction HONO + ȮH = NO_2 + H_2O demonstrates opposite effects on IDT predictions in the Mathieu mechanism compared with the Zhang and Glarborg mechanisms. The major reason for this may be due to the use of different reaction rate coefficients. (4) GRI-Mech 3.0 does not include the HONO species, thus, the sensitivity analysis results demonstrate different characteristics at low temperatures. However, at 1500 K, all mechanisms show very similar sensitivity analysis results. Increasing the reaction rate constants of the H_2 + NO_2

reaction and the decomposition reaction $NO_2 =$ ṄO + Ö significantly increases reactivity, while the three reactions of ṄO with O_2, ȮH and HȮ$_2$ leading to the formation of NO_2 and Ö, Ḣ, and ȮH decrease the reactivity when the rate constants are doubled. To summarize, the HONO species and related reactions have a large effect at low temperatures (< 1200 K), while the transformation reaction between ṄO and NO_2 become important at high temperatures.

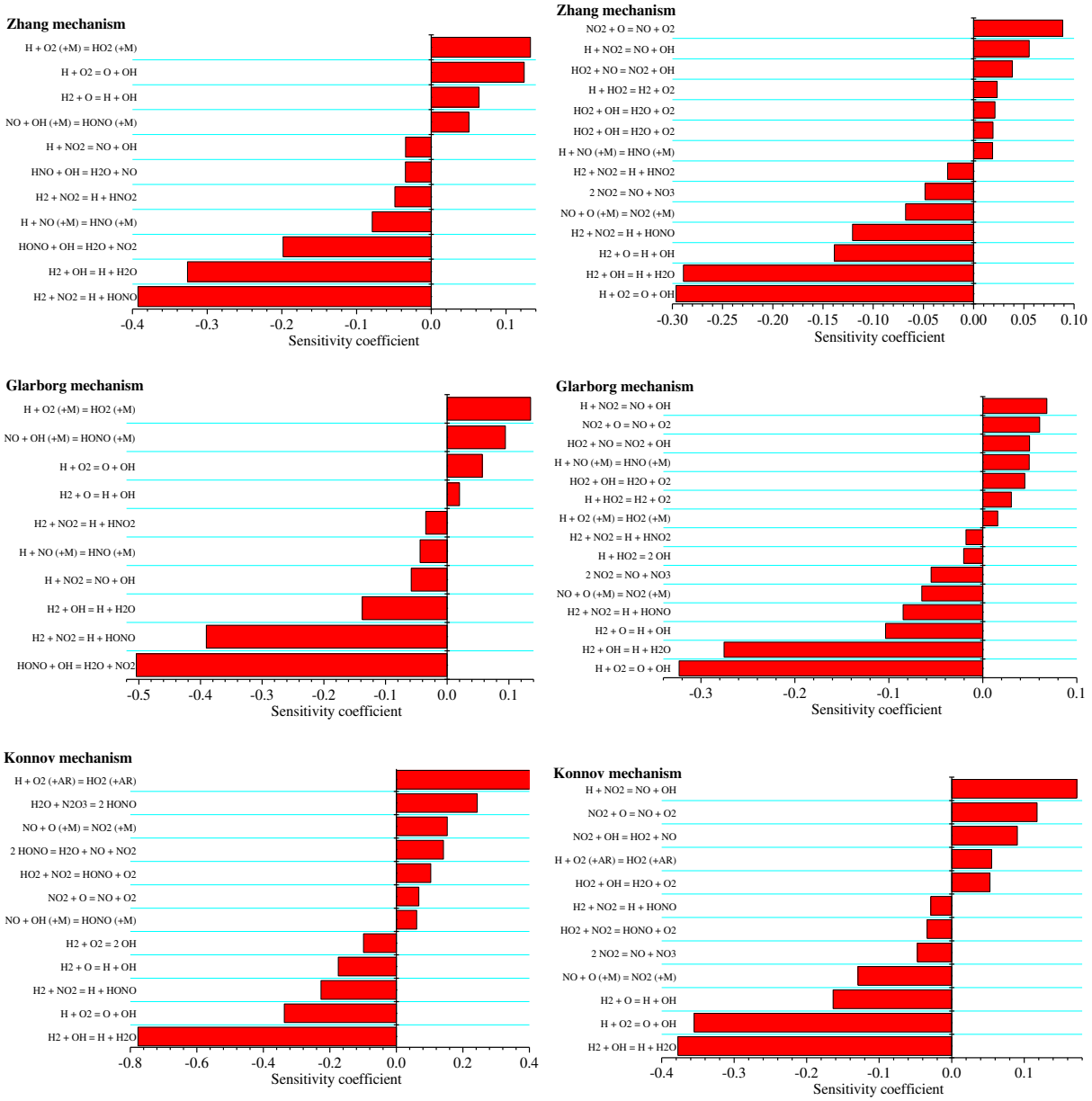

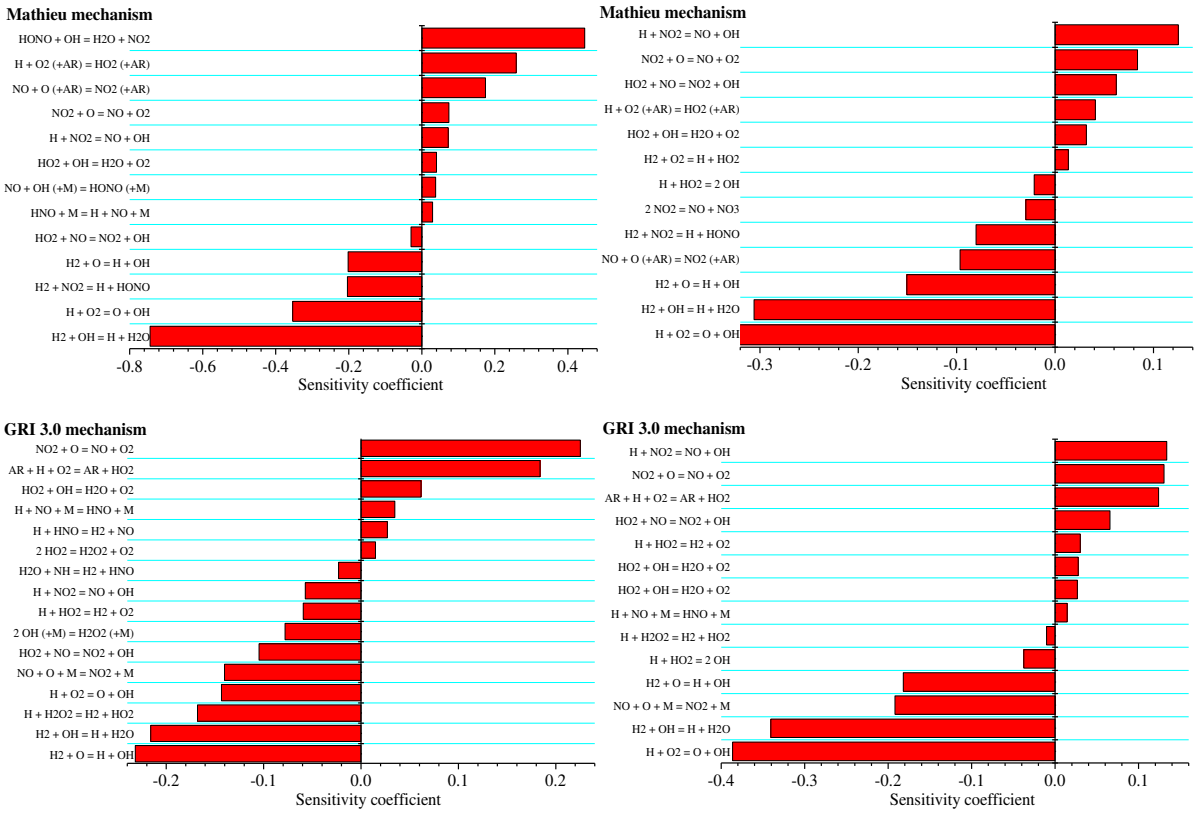

Figure 4. Sensitivity analysis of auto-ignition for H_2/NO_2/Ar mixture (0.01/0.0016/0.9784) by using the five detailed mechanisms at pressure of 20 atm and temperatures of 950 K (left) and 1500 K (right).

Based on systematic flux and sensitivity analyses, the high-temperature chemistry in these detailed mechanisms exhibits small differences, and major differences among these detailed mechanisms lie in the low temperature sub-mechanisms, especially in the HONO and HNO_2 related reactions. Recent interest in advanced combustion engines promotes intense research in low-temperature combustion chemistry involving the NO_x sub-mechanism. To obtain better and more accurate prediction of NO_x chemistry in combustion, high-level theoretical chemistry calculations together with uncertainty minimization methods are employed to obtain more accurate rate constants and uncover unknown reactions using detailed potential energy surface analyses. In an attempt to continuously update detailed mechanisms, key reactions with large uncertainties and new reaction pathways have been updated based on Zhang's mechanism. Table 3 lists the updated reactions

together with their related rate coefficients.

The decomposition reaction of HONO to form ṄO and ȮH is firstly updated with new rate constants, which plays an important role in the formation of ṄO together with the isomerization reaction between HONO and HNO_2. Generally, all of the detailed mechanisms employ this reaction as ṄO + ȮH = HONO. Two sets of reaction rate coefficients from Tsang *et al.*[44] and Fulle *et al.*[45] were employed in the Konnov/Mathieu mechanisms and in the Glarborg mechanism, respectively. The Zhang mechanism adopted the rate coefficients recommended by Atkinson *et al.*[46] with a slight modification of the Troe broadening factor. However, a major drawback of these rate constants was that they were derived at temperatures below 500 K, which were not very relevant to typical combustion conditions. Recently, Chen *et al.*[26] revisited the decomposition reaction kinetics of HONO and HNO_2 using high-level electronic structure calculations coupled with micro-canonical rate theory and the master equation method (RRKM/ME). They computed temperature- and pressure-dependent rate coefficients at temperatures in the range 200–2500 K and at pressures in the range 0.01–100 bar. They compared their computed rate constants with those used in the detailed mechanisms. It was shown that the rate constants used in the Glarborg mechanism exhibited the best agreement within a factor of two compared with their computed results, while the others showed large deviations but were generally within an order of magnitude.

For HNO_2, the Dagaut, Konnov and GRI-Mech 3.0 mechanisms do not include it as a distinct species, while the other mechanisms mainly consider the isomerization reaction between HNO_2 and HONO. Based on high-level theoretical calculations, Chen *et al.*[26] indicated that the decomposition reaction of HNO_2 to ṄO + ȮH was the dominant product channel, which was not considered in all previous detailed mechanisms. Thus, to show the impact of this new reaction and its rate constants

on model performance, the isomerization and decomposition reactions of HNO_2 and HONO are updated and the rate constants are listed in Table 3.

As demonstrated from flux analysis and sensitivity analysis, the reaction $\dot{H} + NO_2 = \dot{N}O + \dot{O}H$ is critical. The rate expression $k(T) = 1.3 \times 10^{14} \exp(-182\ K/T)$ $cm^3\ mol^{-1}\ s^{-1}$ derived by Ko and Fontijn[47] based on high-temperature photochemistry technique at temperatures in the range 296–760 K was employed in all of the detailed mechanisms but was multiplied by a factor of 1.2 in the Zhang mechanism. Su *et al.*[48] extended the temperature range for this reaction to 1100–2000 K by using a shock tube facility and recommended a temperature-independent rate constant as 8.85×10^{13} $cm^3\ mol^{-1}\ s^{-1}$ for $195 \leq T \leq 2000$ K. In 2015, Hass *et al.*[49] replenished experimental results for this reaction for temperatures of 737–882 K in the pressure range 10–20 atm using laminar and turbulent flow reactors, and found a representative rate constant for this reaction of 1.05×10^{14} $cm^3\ mol^{-1}\ s^{-1}$. To minimize the uncertainty in the rate of this reaction, Chen *et al.*[26] proposed a novel strategy to incorporate uncertainty in the minimum energy pathway into an optimization process and obtained a final rate expression, which was in excellent agreement with all of the experimental data.

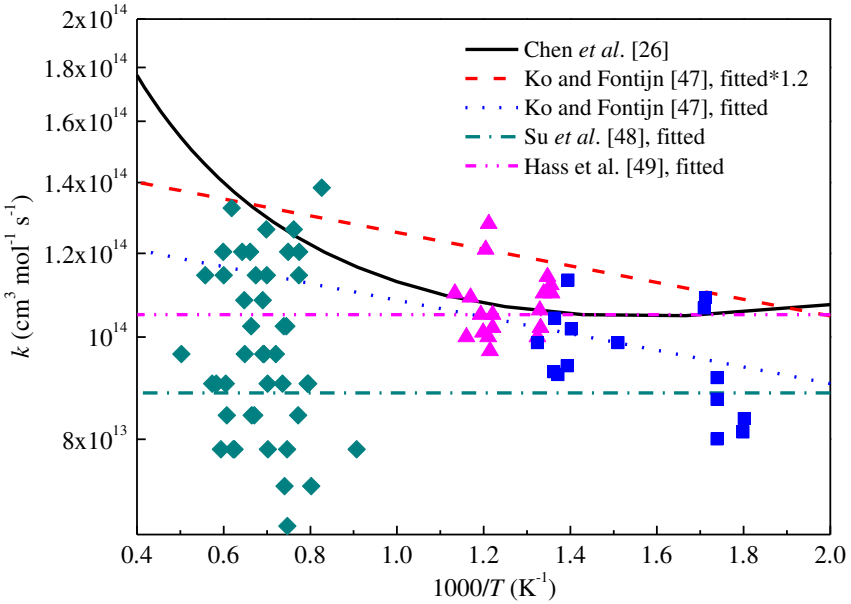

Figure 5. Reaction rate constants for reaction $\dot{H} + NO_2 = \dot{O}H + \dot{N}O$ as a function of temperature. Symbols represents

the corresponding experimental measured rate constants.

Figure 5 demonstrates the rate constants for this reaction as a function of temperature. Although the deviations among these suggested rate constants are not large, the final rate constants optimized by Chen *et al.* [26] exhibits a strong temperature dependence.

Besides the reaction $\dot{H} + NO_2 = \dot{N}O + \dot{O}H$, the abstraction reaction of H_2 and NO_2 to form $\dot{N}O$ and H_2O also shows large sensitivity coefficients. The recent high-level theoretical calculations by Chai *et al.*[25] for this abstraction reaction were employed in the Zhang and Glarborg mechanisms and adopted in this work. The reaction $HONO + \dot{O}H = H_2O + NO_2$ represents a major consumption pathway for HONO and also shows a large sensitivity coefficient at low temperature conditions, but this reaction exhibits an opposite sensitivity coefficient in the Mathieu mechanism compared with the other three mechanisms as shown in Figure 6. The rate constant employed in the Mathieu mechanism increases with increasing temperature, while the rate constants used in the other three mechanisms[50] exhibit a slight negative temperature dependence. Theoretical calculations for this reaction[51] also indicated a negative temperature dependence at temperatures below 1000 K, which correlates with the experimental results.[50] In this work the reactions between $\dot{H}$ and HONO are also updated using the theoretical calculations of Chai *et al.*[25]

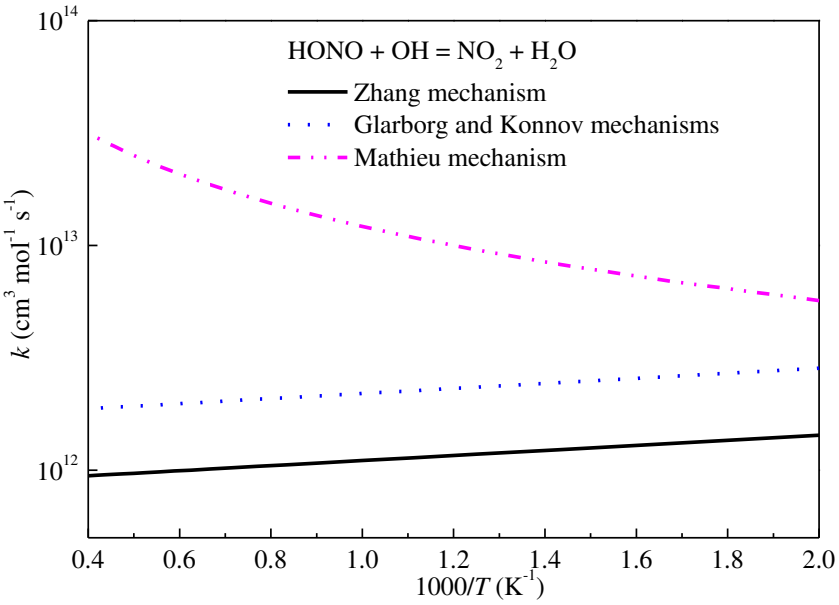

Figure 6. Reaction rate constants used for reaction HONO + ȮH = H_2O + NO_2 as a function of temperature.

Although the reaction reactivity of H_2/NO_2/Ar mixture is not sensitive to the reactions relevant to HNO according to our sensitivity analysis, nevertheless the HNO species plays a critical role in the formation of NO_x and in the oxidation of ammonia. The reactions between HNO and ȮH have been updated with theoretical calculated rate coefficients.[27] In addition, the reaction HNO + NO_2 = ṄO + HONO involving the inter-conversion of ṄO and NO_2 was found to be important in the oxidation of nitromethane CH_3NO_2, and was theoretically studied at the G4 level of theory by Shang *et al.*[52] Their calculated rate expression has been used in our updated mechanism.

The reactions H_2NO + O_2 = HNO + HȮ$_2$ and HNO + O_2 = ṄO + HȮ$_2$ are major consumption steps for H_2NO and HNO. The first reaction was studied theoretically by Song *et al.*,[19, 53] and the activation energy was slightly decreased within the estimated uncertainty to facilitate modeling predictions of ammonia oxidation and thermal DeNO$_x$ at high oxygen concentrations.[19] The rate expression calculated by Song has been adopted here. However, for the reaction HNO + O_2 = ṄO + HȮ$_2$, no experimental or theoretical results were found, and the estimated rate constants from QRRK theory[37] were adopted in previous mechanisms. To minimize the uncertainty of this reaction, its rate

constants have been calculated here using high-level quantum chemistry calculations together with transition state theory. Specifically, geometry optimization and hindered rotor scan analyses are performed at the B2PLYP-D3/aug-cc-pVTZ level of theory.[54] Geometry optimization at this level can approach the accuracy of CCSD(T)/cc-pVTZ level.[55] Single-point energies are refined at the CCSD(T) level with aug-cc-pVTZ and aug-cc-pVQZ basis sets and then extrapolated to the complete basis set (CBS) limit.[56, 57] For all the species calculated with open-shell CCSD(T) method, all T1 diagnostics values[58] are within 0.035, indicating that single-reference CCSD(T) method is adequate for this reaction.[55, 59] The energy barrier at the CCSD(T)/CBS level is 14.68 kcal mol^{-1} and Eckart tunneling corrections[60] are included in the calculation. The rate constants are calculated in the temperature range 500–2500 K with 100 K increments using MultiWell software[61] and fitted to the modified Arrhenius expression. The rate constants for this reaction as a function of temperature are plotted in Figure 7. It can be seen that the rate constants used by Konnov and Mathieu are different from those used in the Zhang and Glarborg mechanisms. The computed rate constants in this work are lower than those used in the Zhang and Glarborg mechanisms at temperatures below 1000 K. Moreover, as the initial major consumption reactions of NH_3, the abstraction reactions by Ḣ atoms and ȮH radicals were theoretically investigated by Nguyen and Stanton[62, 63] by combining the high-accuracy extrapolated ab initio thermochemistry (HEAT) protocol with semi-classical transition state theory (SCTST). The computed results for NH_3 + Ḣ were found to be in good correlation with the experimental results of Michael *et al.*,[64] which were employed in detailed mechanisms. The calculated and fitted rate constants for NH_3 + ȮH by Nguyen *et al.*[62] slightly deviate from the previous results, but the overall deviations are within 30%. The computed and fitted rate coefficients by Nguyen *et al.*[62, 63] extend the temperature ranges and are employed in the updated mechanism.

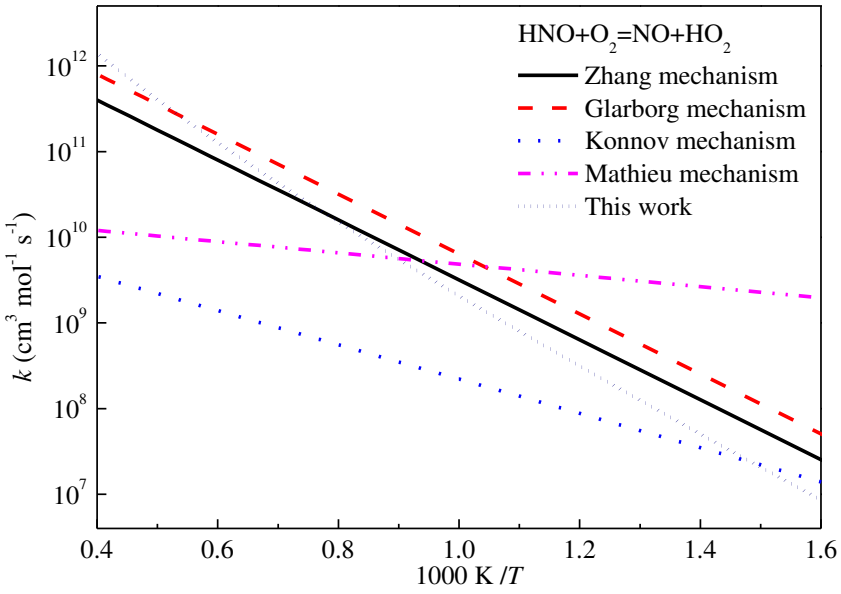

Figure 7. Reaction rate constants for reaction HNO + O_2 = ṄO + HȮ$_2$ as a function of temperature.

Table 3. Updated reactions and the corresponding reaction rate coefficients.

	Reaction		Rate coefficient (cm, mol, s, cal)			Source
		p / atm	*A*	*n*	*E*	
1	HNO_2 = HONO	0.01	3.26×10^{34}	–7.97	45490.	26
		0.10	2.77×10^{33}	–7.58	45250.	
		0.316	1.93×10^{32}	–7.18	44940.	
		1.00	1.56×10^{30}	–6.47	44360.	
		3.16	2.17×10^{27}	–5.49	43670.	
		10.0	4.68×10^{24}	–4.52	43320.	
		31.6	1.14×10^{23}	–3.81	43640.	
		100.0	2.03×10^{22}	–3.35	44430.	
2	ȮH + ṄO = HONO	0.01	5.02×10^{21}	–4.24	899.	26
		0.10	5.31×10^{22}	–4.24	1184.	
		0.316	1.38×10^{23}	–4.22	1376.	
		1.00	3.09×10^{23}	–4.17	1621.	
		3.16	5.45×10^{23}	–4.09	1911.	
		10.0	6.35×10^{23}	–3.97	2222.	
		31.6	3.68×10^{23}	–3.75	2501.	
		100.0	7.29×10^{22}	–3.41	2660.	
3	ȮH + ṄO = HNO_2	0.01	3.16×10^{18}	–3.74	1405.	26
		0.10	3.03×10^{18}	–3.43	2618.	
		0.316	2.23×10^{18}	–3.24	3248.	
		1.00	1.43×10^{18}	–3.03	3899.	
		3.16	6.91×10^{17}	–2.79	4535.	
		10.0	2.04×10^{17}	–2.49	5125.	

		31.6	3.07×10^{16}	–2.12	5648.	
		100.0	1.95×10^{15}	–1.64	6099.	
4	$\dot{H} + NO_2 = \dot{O}H + \dot{N}O$		2.01×10^{11}	0.84	–1058.	26
5	$\dot{H} + HONO = \dot{N}O + H_2O$	0.01	3.91×10^{09}	0.99	4049.	27
		0.10	3.93×10^{09}	0.99	4049.	
		0.316	3.97×10^{09}	0.99	4051.	
		1.00	4.30×10^{09}	0.98	4070.	
		3.16	7.04×10^{09}	0.92	4225.	
		10.0	2.60×10^{10}	0.76	4736.	
		31.6	7.91×10^{10}	0.64	5519.	
		100.0	2.79×10^{10}	0.80	6146.	
6	$\dot{H} + HONO = H_2 + NO_2$		1.89×10^{03}	2.83	1423.	27
7	$\dot{H} + HNO_2 = H_2 + NO_2$		2.33×10^{04}	2.77	–2022.	27
8	$\dot{H} + HNO_2 = \dot{N}O + H_2O$	0.01	3.39×10^{09}	1.07	5568.	27
		0.10	3.39×10^{09}	1.07	5567.	
		0.316	3.39×10^{09}	1.07	5567.	
		1.00	3.38×10^{09}	1.07	5565.	
		3.16	3.38×10^{09}	1.07	5560.	
		10.0	3.40×10^{09}	1.07	5546.	
		31.6	4.32×10^{09}	1.04	5591.	
		100.0	1.27×10^{10}	0.91	5968.	
9	$\dot{H} + HNO_2 = HNO + \dot{O}H$	0.01	3.61×10^{07}	1.78	5565.	27
		0.10	3.61×10^{07}	1.78	5566.	
		0.316	3.62×10^{07}	1.78	5567.	
		1.00	3.65×10^{07}	1.78	5570.	
		3.16	3.74×10^{07}	1.77	5580.	
		10.0	4.14×10^{07}	1.76	5617.	
		31.6	6.23×10^{07}	1.71	5770.	
		100.0	1.81×10^{08}	1.59	6233.	
10	$HNO + \dot{O}H = \dot{H} + HONO$	0.01	1.06×10^{03}	2.76	4439.	27
		0.10	1.09×10^{03}	2.75	4450.	
		0.316	1.18×10^{03}	2.74	4476.	
		1.00	1.48×10^{03}	2.72	4554.	
		3.16	2.71×10^{03}	2.64	4768.	
		10.0	9.67×10^{03}	2.49	5253.	
		31.6	5.31×10^{04}	2.29	6063.	
		100.0	1.03×10^{05}	2.24	6951.	
11	$HNO + \dot{O}H = \dot{N}O + H_2O$	0.01	5.82×10^{10}	0.40	3762.	27
		0.10	5.85×10^{10}	0.40	3763.	
		0.316	5.92×10^{10}	0.40	3764.	
		1.00	6.30×10^{10}	0.39	3782.	
		3.16	9.53×10^{10}	0.34	3931.	

		10.0	2.60×10^{11}	0.23	4413.	
		31.6	3.83×10^{11}	0.20	5099.	
		100.0	4.18×10^{10}	0.51	5532.	
12	$HNO + NO_2 = \dot{N}O + HONO$		7.85×10^{02}	3.06	3882.	52
13	$HNO + O_2 = \dot{N}O + H\dot{O}_2$		3.99×10^{05}	2.30	14605.	this work
14	$N_2O+H_2 = N_2+H_2O$		7.00×10^{12}	0.00	32500.	42
15	$NH_3 + \dot{O}H = NH_2 + H_2O$		4.30×10^{03}	2.83	–431.	62
16	$NH_3 + \dot{H} = NH_2 + H_2$		2.89×10^{06}	2.23	10406.	63
17	$H_2NO + O_2 = HNO + H\dot{O}_2$		2.30×10^{02}	2.99	16500.	19, 53

3.4. Skeletal reduction results

During the skeletal reduction process, the size of the skeletal mechanism is controlled by a threshold value, and the resulting skeletal mechanisms at different threshold values can be validated by comparing their model performance with the detailed mechanism. Starting from the updated detailed mechanism consisting of 44 species and 252 reactions, a skeletal mechanism with 28 species and 163 reactions is obtained using the DRGEP method at a threshold value of 0.4 and the predicted relative errors of ignition under sampling conditions are within 10%. To further reduce the number of species, we also perform a second-stage skeletal reduction via the DRGEP method, but it is hard to remove any species within the same error range. The resulting 28 species mechanism is further reduced via the ISSA method, and a final skeletal mechanism with 27 species and 130 reactions is obtained. The species H_2NN and its related reactions are deleted at this stage, also indicating that a single skeletal reduction is usually not enough to derive a minimal skeletal mechanism.[35] Table 1 lists the retained species in the final skeletal mechanism relevant to the NO_x sub-mechanism, and the HOĊO species has been removed compared with the syngas sub-mechanism in the detailed mechanism. It was shown by Nilsson and Konnov[65] that this species and its related chemistry were in fact not important to any significant extent under a wide range of combustion conditions for syngas with different compositions of H_2 and CO.

Based on reaction pathway and sensitivity analyses, it can be concluded that, although the species and reactions in different detailed mechanisms show large differences, most of the species and reactions have little effect on mechanism performance. When considering the retained species and reactions in the skeletal mechanism compared to the detailed one, it is found that the small set of reactions controlling the major reaction pathways and affecting the predictive capability of the detailed mechanism are the same, and the different performance relies in the selection of rate constants for this small set of reactions. The reduction in computational cost of the skeletal mechanism was measured for both the homogeneous ignition and diffusive flame systems. It is found that there is approximately a 60% CPU-time reduction for ignition and JSR species profile simulations and a 40% reduction for laminar simulations using the skeletal mechanism.

3.5. Performance of the developed mechanism

The updated detailed mechanism and the reduced skeletal mechanism for syngas/NO_x have been validated against typical experimental data including IDTs and species profiles. A series of experimental investigations on nitrogen chemistry relevant to the syngas oxidation process have been reported in the last few decades as summarized by Glarborg *et al*.[19] and Zhang *et al*.[20] IDTs for $H_2/NO_2/O_2/Ar$, $H_2/N_2O/O_2/Ar$, and $NH_3/O_2/Ar$ mixtures are selected as the primary major targets for validation since they can cover a wide range of pressures and temperatures.

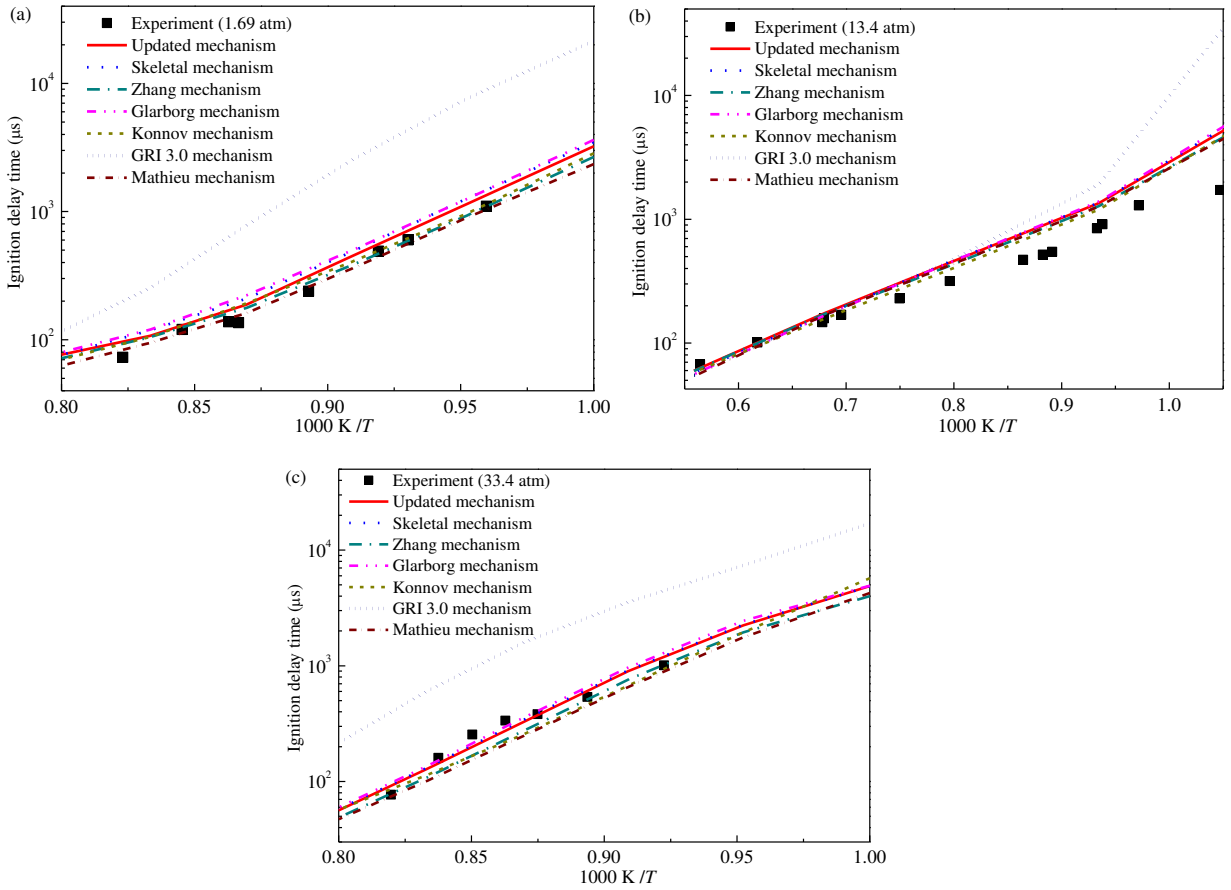

Figure 8. Ignition delay times from shock tube experiments[41] in comparison to model predictions for $0.0133H_2/0.0067O_2/0.0001NO_2/0.9799Ar$ mixtures (mole fraction) at different pressures.

To improve the predictability of NO_x mechanism, the effect of NO_x addition on the combustion properties of fuel oxidation system have been widely studied. Mathieu *et al.*[41] measured ignition delay times of $H_2/O_2/NO_2$ mixtures in a shock tube behind reflected shock waves. Figure 8 illustrates the experimental data with simulations using the updated detailed and skeletal mechanisms as well as the other five detailed mechanisms. One can see that all of the mechanisms considered, except GRI-Mech 3.0, exhibit similar and good performance. The reduced skeletal mechanism reproduces the simulation results in good agreement with the detailed one. The major reason for the poor performance of GRI-Mech 3.0 is the omission of the HONO species because NO_2 is mostly converted to $\dot{N}O$ by the reaction $\dot{H} + NO_2 = \dot{N}O + \dot{O}H$, which is included in all mechanisms and the adopted

rate constants also show small differences. GRI-Mech 3.0 can still predict some reasonable ignition delay time since the HONO related reactions mainly affect IDTs at low temperature conditions as illustrated by Figure 4.

The $H_2/N_2O/O_2$ reaction system is considered as another target to explore the interaction of hydrogen and NO_x and validate the performances of different mechanisms. Mathieu *et al.*[40] conducted shock tube studies on the effect of N_2O addition on the ignition of the H_2/O_2 system over a wide range of temperatures (940–1675 K) and pressures (1.6, 13 and 32 atm), and recently Mulvihill *et al.*[42] performed a shock tube study on the less-dilute H_2/N_2O reaction system. They recommended new rate constants for the reaction $H_2 + N_2O = N_2 + H_2O$, which is used in the updated mechanism. Figure 9 shows IDTs from shock tube experiments for the H_2/N_2O reaction systems together with modeling results. It can be seen that the updated and skeletal mechanisms exhibit better performance compared to the other mechanisms. For the less-dilute H_2/N_2O system shown in Figure 9(d), the updated mechanism shows an improved performance using the rate constants recommended by Mulvihill *et al.*[42] for the reaction $H_2 + N_2O = N_2 + H_2O$.

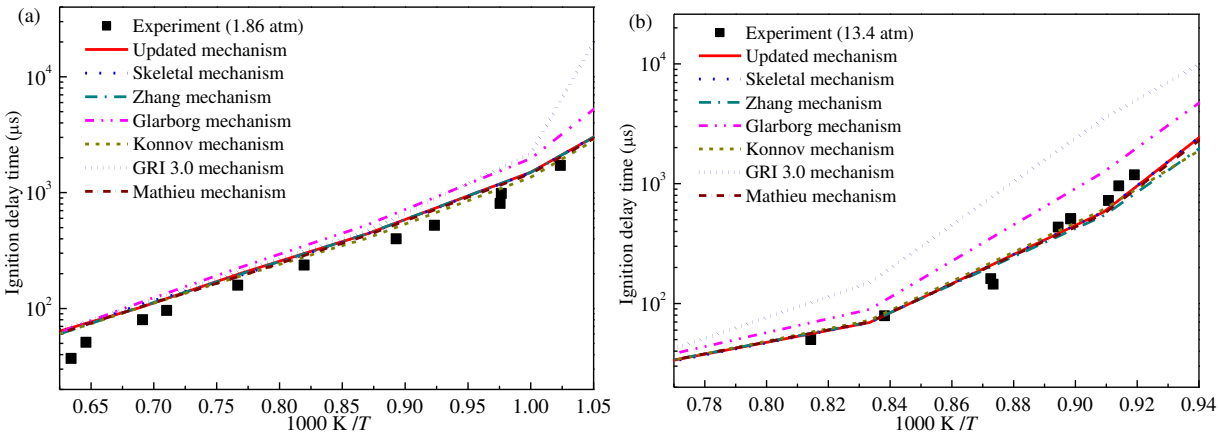

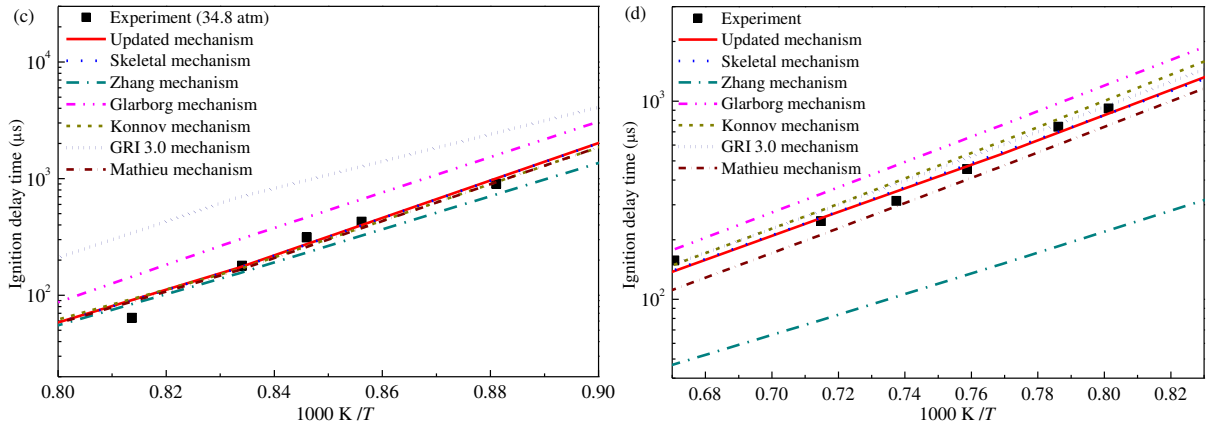

Figure 9. Ignition delay times from shock tube experiments in comparison to model predictions for $0.01H_2/0.01O_2/0.0032N_2O/0.9768Ar$ mixtures (mole fraction) at different pressures[40] (a)–(c) and for $0.10H_2/0.10N_2O/0.80Ar$ mixture at 0.68 atm[42] ((d)).

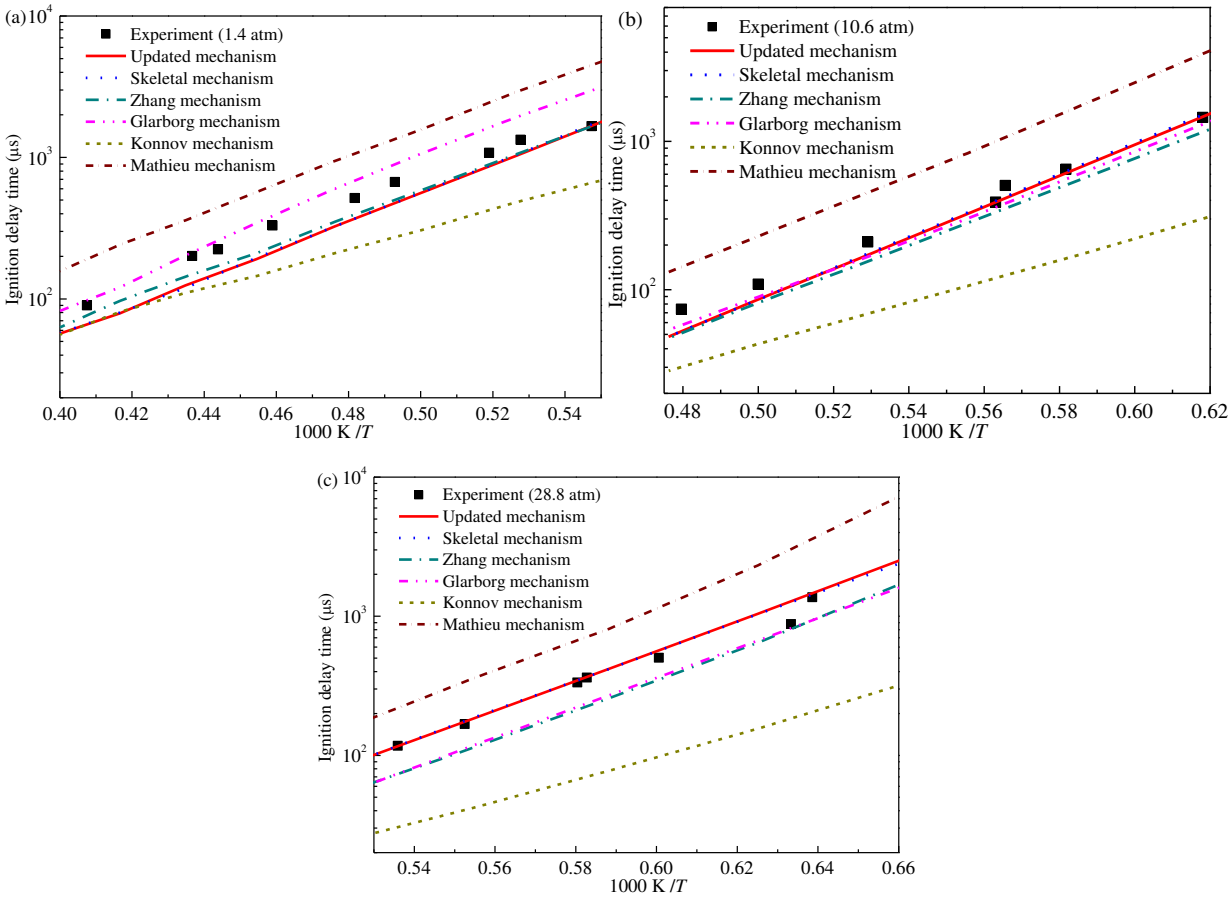

Figure 10. Ignition delay times from shock tube experiments[66] in comparison to model predictions for $0.01143NH_3/0.00857O_2/0.98Ar$ mixtures (mole fraction) at different pressures.

Figure 10 shows IDTs for $NH_3/O_2/Ar$ mixtures at different pressures obtained from shock tube

experiments[66] together with modeling results. The updated detailed and reduced skeletal mechanisms show improved predictions, especially at high pressure conditions. Figure 11 shows sensitivity analysis results for NH_3/O_2/Ar mixture using the updated detailed mechanism at 20 atm pressure and 1500 K. It can be seen that the reactions related to H_2NO and HNO species are very important. The reactions of these two species with O_2 exhibit large sensitivity coefficients. By employing high-level theoretical calculation results together with abstraction reactions of NH_3 by Ḣ atoms and ȮH radicals as shown in Table 3, the updated detailed mechanism shows better performance in predicting IDTs for these NH_3/O_2/Ar mixtures.

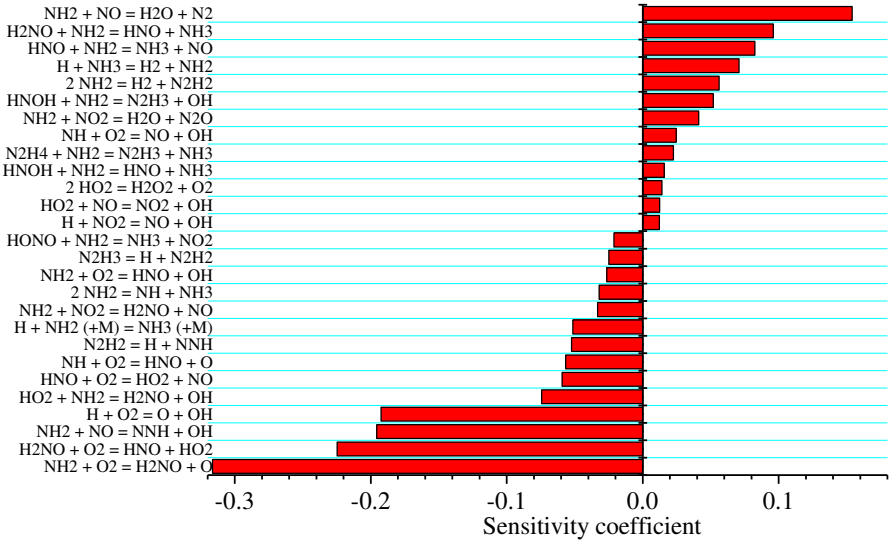

Figure 11. Sensitivity analysis of auto-ignition for NH_3/O_2/Ar mixture by using the updated detailed mechanisms at pressure of 20 atm and temperature of 1500 K.

Species concentration profiles from Jet-stirred reactors (JSR) and Flow reactor (FR) experiments are another important target to validate a detailed mechanism for nitrogen chemistry and NO_x emission prediction. The FR experiment designed by Abian *et al.*[67] provided a benchmark dataset for the prediction of thermal ṄO. This mechanism is controlled by the reaction N_2 + Ö = ṄO + N, and the rate constants employed in all of the mechanisms show small differences. Thus, the predicted ṄO

concentrations using the considered detailed mechanisms are very similar to one another. Figure 12 demonstrates a typical experimental JSR species profiles by Dayma and Dagaut[68] and the predicted results. The updated and skeletal mechanism together with the Zhang and Glarborg mechanisms exhibit better performances compared with the other mechanisms. GRI-Mech 3.0 is outdated due to the lack of many key species relevant to low-temperature nitrogen chemistry. As shown in Table 3, major updates in the current mechanism and the differences among previous mechanisms lie in the low-temperature chemistry, especially for HONO and HNO_2 related reactions. To demonstrate the difference and analyze the impact of the new reaction pathway on model performance, a rate-of-production (ROP) analysis is performed for the $H_2/O_2/N_2$ mixture perturbed by $\dot{N}O$ using the updated mechanism together with the Zhang and Glarborg mechanisms at 30 atm and 850 K, Figure 13. The major reactions controlling the transformation of $\dot{N}O$ and NO_2 are the same but with different rate constants. However, by incorporating the latest identified decomposition reaction of HNO_2,[26] it can be seen that the unimolecular decomposition reaction of HNO_2 to directly generate $\dot{O}H$ and $\dot{N}O$ is favored over the isomerization reaction.

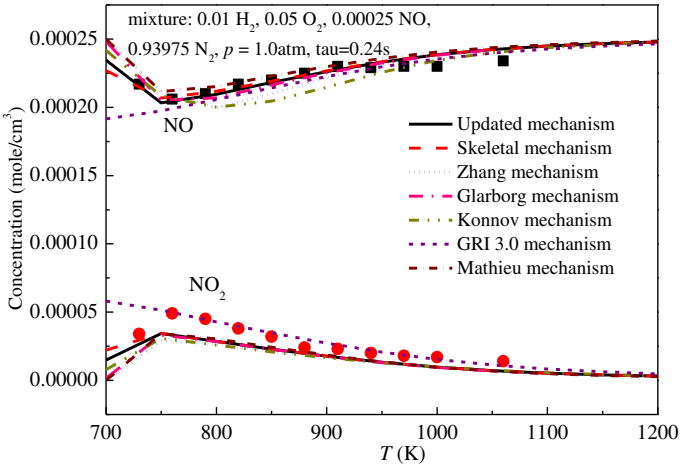

Figure 12. $\dot{N}O$ and NO_2 species profiles as a function of temperature from experiment and modeling results. Symbols represent experimental measurements.[68]

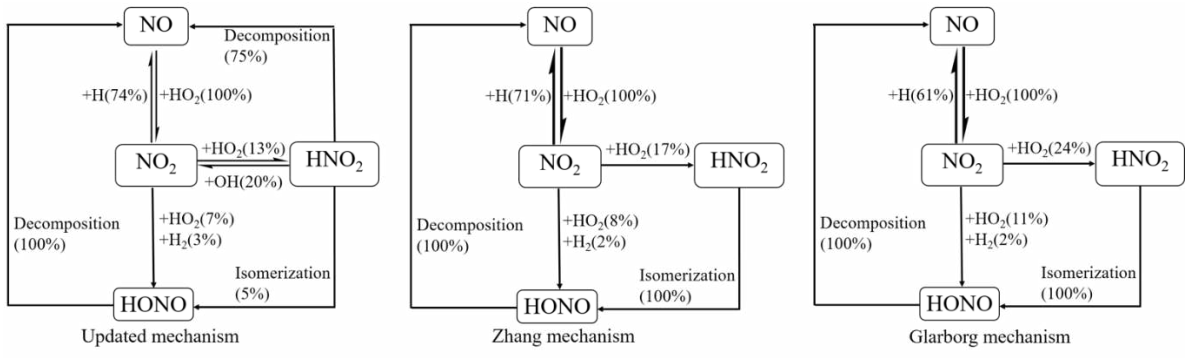

Figure 13. ROP analysis for NO species during JSR simulations for 0.01 H_2/0.05 O_2/0.93975 N_2/0.00025 NO mixture with residence time of 0.24 sec at 30 atm and 850 K.

Finally, to further validate the updated detailed and skeletal mechanisms, laminar flame speeds for H_2/N_2O mixture diluted by 60% Ar measured by Mével *et al.*[69] are used to test the mechanism performance. Figure 14 shows the predicted laminar flame speeds as a function of equivalence ratio compared with experimental results at pressure of 1 atm and initial temperature of 300 K. It can be seen that the skeletal mechanism also exhibits high-fidelity in prediction of laminar flame speed compared with the detailed mechanism and experimental results.

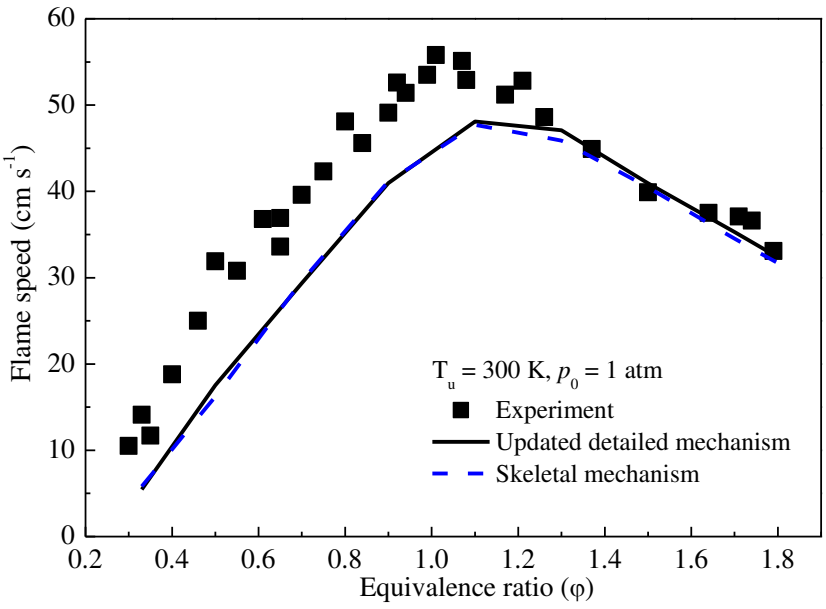

Figure 14. Laminar flame speed comparisons between experimental data and mechanism predictions for H_2/N_2O mixture diluted by 60% Ar at 1.0 atm and 300 K.

4. Conclusions

In spite of the apparent simplicity of the syngas/NO_x reaction system, available detailed mechanisms describing it still exhibit different performances in predicting combustion properties and NO_x emissions. To clarify the differences among various detailed mechanisms, we have performed a comparative chemical kinetic analysis by using flux and sensitivity analyses for five available detailed mechanisms describing the syngas/NO_x system. An updated detailed mechanism has been developed by incorporating recent theoretical advancements of several important elementary reactions. The main conclusions of the present study are summarized as follows.

(1) The species relevant to nitrogen chemistry included in different detailed mechanisms for syngas combustion are different, and none of the selected detailed mechanisms are comprehensive enough to contain all of the species. Naturally, the recently developed detailed mechanisms such as the Zhang and Glarborg mechanisms are more comprehensive than the earlier ones.

(2) Although the species and reactions included in various detailed mechanisms show large differences, the major reaction pathways and overall mechanism performances are affected by a small number of species and reactions based on flux and sensitivity analyses. The thermal $\dot{N}O$ formation mechanism in contemporary detailed mechanisms is identical and only small deviations exist in rate constants. Major differences among the detailed mechanisms lie in the low-temperature sub-mechanism, especially for the reactions related to HONO and HNO_2.

(3) The rate constants for reaction $HNO + O_2 = \dot{N}O + H\dot{O}_2$ are calculated at the CCSD(T)/CBS level of theory together with TST and Eckart tunneling correction. With recent advancement in several important reactions, an updated detailed mechanism has been developed and validated. The updated mechanism incorporates new reaction pathways and exhibits a better performance

for a series of conditions, especially at high-pressure conditions.

(4) A reduced skeletal mechanism is obtained using a combination of the DRGEP and ISSA methods, and the skeletal mechanism, which can be coupled with CFD simulations, exhibits a high-fidelity performance compared to the detailed one.

Supporting Information

The Supporting Information is available free of charge on the ACS Publications website.

The updated detailed and skeletal mechanisms; thermodynamic and transport properties.

Acknowledgments

Q.-D. Wang and Y. Sun would like to acknowledge financial funding by the China Scholarship Council (CSC). The authors want to acknowledge financial support of Science Foundation Ireland under Grant Nos. 15/IA/3177 and 16/SP/3829 and also the National Natural Science Foundation of China (21403296). The Computational resources are provided by the Irish Centre for High-End Computing (ICHEC), under project number ngche064c and ngche073c.

References

1. Ahmed, U.; Zahid, U.; Lee, Y., Process simulation and integration of IGCC systems for H-2/syngas/electricity generation with control on CO2 emissions. *Int. J. Hydrogen Energy* **2019,** 44, (14), 7137-7148.

2. Ge, H. J.; Zhang, H. F.; Guo, W. J.; Song, T.; Shen, L. H., System simulation and experimental verification: Biomass-based integrated gasification combined cycle (BIGCC) coupling with chemical looping gasification (CLG) for power generation. *Fuel* **2019,** 241, 118-128.

3. Ryzhkov, A.; Bogatova, T.; Gordeev, S., Technological solutions for an advanced IGCC plant. *Fuel* **2018,** 214, 63-72.

4. Curran, H. J., Developing detailed chemical kinetic mechanisms for fuel combustion. *Proc. Combust. Inst.* **2019,** 37, (1), 57-81.

5. Lu, T. F.; Law, C. K., Toward accommodating realistic fuel chemistry in large-scale computations. *Prog. Energy Combust. Sci.* **2009,** 35, (2), 192-215.

6. O Conaire, M.; Curran, H. J.; Simmie, J. M.; Pitz, W. J.; Westbrook, C. K., A comprehensive modeling study of hydrogen oxidation. *Int. J. Chem. Kinet.* **2004,** 36, (11), 603-622.

7. Konnov, A. A., Yet another kinetic mechanism for hydrogen combustion. *Combust. Flame* **2019,** 203, 14-22.

8. Konnov, A. A., Remaining uncertainties in the kinetic mechanism of hydrogen combustion. *Combust. Flame* **2008,**

152, (4), 507-528.
9. Hong, Z. K.; Davidson, D. F.; Hanson, R. K., An improved H-2/O-2 mechanism based on recent shock tube/laser absorption measurements. *Combust. Flame* **2011,** 158, (4), 633-644.
10. Keromnes, A.; Metcalfe, W. K.; Heufer, K. A.; Donohoe, N.; Das, A. K.; Sung, C. J.; Herzler, J.; Naumann, C.; Griebel, P.; Mathieu, O.; Krejci, M. C.; Petersen, E. L.; Pitz, W. J.; Curran, H. J., An experimental and detailed chemical kinetic modeling study of hydrogen and syngas mixture oxidation at elevated pressures. *Combust. Flame* **2013,** 160, (6), 995-1011.
11. Varga, T.; Nagy, T.; Olm, C.; Zsely, I. G.; Palvolgyi, R.; Valko, E.; Vincze, G.; Cserhati, M.; Curran, H. J.; Turanyi, T., Optimization of a hydrogen combustion mechanism using both direct and indirect measurements. *Proc. Combust. Inst.* **2015,** 35, 589-596.
12. Miller, J. A.; Bowman, C. T., Mechanism and Modeling of Nitrogen Chemistry in Combustion. *Prog. Energy Combust. Sci.* **1989,** 15, (4), 287-338.
13. Konnov, A. A., Implementation of the NCN pathway of prompt-NO formation in the detailed reaction mechanism. *Combust. Flame* **2009,** 156, (11), 2093-2105.
14. Mathieu, O.; Giri, B.; Agard, A. R.; Adams, T. N.; Mertens, J. D.; Petersen, E. L., Nitromethane ignition behind reflected shock waves: Experimental and numerical study. *Fuel* **2016,** 182, 597-612.
15. Ahmed, S. F.; Santner, J.; Dryer, F. L.; Padak, B.; Farouk, T. I., Computational Study of NOx Formation at Conditions Relevant to Gas Turbine Operation, Part 2: NOx in High Hydrogen Content Fuel Combustion at Elevated Pressure. *Energy Fuels* **2016,** 30, (9), 7691-7703.
16. Frassoldati, A.; Faravelli, T.; Ranzi, E., The ignition, combustion and flame structure of carbon monoxide/hydrogen mixtures. Note 1: Detailed kinetic modeling of syngas combustion also in presence of nitrogen compounds. *Int. J. Hydrogen Energy* **2007,** 32, (15), 3471-3485.
17. Santner, J.; Ahmed, S. F.; Farouk, T.; Dryer, F. L., Computational Study of NOx Formation at Conditions Relevant to Gas Turbine Operation: Part 1. *Energy Fuels* **2016,** 30, (8), 6745-6755.
18. Dagaut, P.; Glarborg, P.; Alzueta, M. U., The oxidation of hydrogen cyanide and related chemistry. *Prog. Energy Combust. Sci.* **2008,** 34, (1), 1-46.
19. Glarborg, P.; Miller, J. A.; Ruscic, B.; Klippenstein, S. J., Modeling nitrogen chemistry in combustion. *Prog. Energy Combust. Sci.* **2018,** 67, 31-68.
20. Zhang, Y. J.; Mathieu, O.; Petersen, E. L.; Bourque, G.; Curran, H. J., Assessing the predictions of a NOx kinetic mechanism on recent hydrogen and syngas experimental data. *Combust. Flame* **2017,** 182, 122-141.
21. Sirumalla, S. K.; Mayer, M. A.; Niemeyer, K. E.; West, R. H., Assessing impacts of discrepancies in model parameters on autoignition model performance: A case study using butanol. *Combust. Flame* **2018,** 190, 284-292.
22. Boivin, P.; Sanchez, A. L.; Williams, F. A., Four-step and three-step systematically reduced chemistry for wide-range H-2-air combustion problems. *Combust. Flame* **2013,** 160, (1), 76-82.
23. Boivin, P.; Williams, F. A., Extension of a wide-range three-step hydrogen mechanism to syngas. *Combust. Flame* **2018,** 196, 85-87.
24. Li, R.; He, G. Q.; Qin, F.; Pichler, C.; Konnov, A. A., Comparative analysis of detailed and reduced kinetic models for CH4 + H-2 combustion. *Fuel* **2019,** 246, 244-258.
25. Chai, J. J.; Goldsmith, C. F., Rate coefficients for fuel + NO2 : Predictive kinetics for HONO and HNO2 formation. *Proc. Combust. Inst.* **2017,** 36, (1), 617-626.
26. Chen, X.; Fuller, M. E.; Goldsmith, C. F., Decomposition kinetics for HONO and HNO2. *Reaction Chemistry & Engineering* **2019,** 4, (2), 323-333.
27. Fuller, M. E.; Goldsmith, C. F., On the relative importance of HONO versus HNO2 in low-temperature combustion. *Proc. Combust. Inst.* **2019,** 37, (1), 695-702.

28. Smith, G. P.; Golden, D. M.; Frenklach, M.; Moriarty, N. W.; Eiteneer, B.; Goldenberg, M.; Bowman, C. T.; Hanson, R. K.; Song, S.; Gardiner Jr, W. C., *GRI 3.0 Mechanism,* http://combustion.berkeley.edu/gri-mech/releases.html **1999**.
29. Cathonnet, M.; Boettner, J.-C.; James, H., Etude expérimentale et simulation de la pyrolyse du methanol. *J. Chim. Phys.* **1979,** 76, 183-189.
30. Wang, Q. D.; Fang, Y. M.; Wang, F.; Li, X. Y., Systematic analysis and reduction of combustion mechanisms for ignition of multi-component kerosene surrogate. *Proc. Combust. Inst.* **2013,** 34, 187-195.
31. Pepiot-Desjardins, P.; Pitsch, H., An efficient error-propagation-based reduction method for large chemical kinetic mechanisms. *Combust. Flame* **2008,** 154, (1-2), 67-81.
32. Mauersberger, G., ISSA (iterative screening and structure analysis) - a new reduction method and its application to the tropospheric cloud chemical mechanism RACM/CAPRAM2.4. *Atmos. Environ.* **2005,** 39, (23-24), 4341-4350.
33. Xia, A. G.; Michelangeli, D. V.; Makar, P. A., Mechanism reduction for the formation of secondary organic aerosol for integration into a 3-dimensional regional air quality model: alpha-pinene oxidation system. *Atmos. Chem. Phys.* **2009,** 9, (13), 4341-4362.
34. Wang, Q. D.; Fang, Y. M.; Wang, F.; Li, X. Y., Skeletal mechanism generation for high-temperature oxidation of kerosene surrogates. *Combust. Flame* **2012,** 159, (1), 91-102.
35. Wang, Q. D., Skeletal Mechanism Generation for Methyl Butanoate Combustion via Directed Relation Graph Based Methods. *Acta Physico-Chimica Sinica* **2016,** 32, (3), 595-604.
36. Metcalfe, W. K.; Burke, S. M.; Ahmed, S. S.; Curran, H. J., A Hierarchical and Comparative Kinetic Modeling Study of C-1 - C-2 Hydrocarbon and Oxygenated Fuels. *Int. J. Chem. Kinet.* **2013,** 45, (10), 638-675.
37. Dean, A. M.; Bozzelli, J. W., Combustion chemistry of nitrogen. In *Gas-phase combustion chemistry*, Springer: 2000; pp 125-341.
38. Diau, E. W. G.; Lin, M. C., Theoretical-Study of H(D)+N2O - Effects of Pressure, Temperature, and Quantum-Mechanical Tunneling on H(D)-Atom Decay and Oh(D)-Radical Production. *J. Phys. Chem.* **1995,** 99, (17), 6589-6594.
39. Klippenstein, S. J.; Harding, L. B.; Glarborg, P.; Miller, J. A., The role of NNH in NO formation and control. *Combust. Flame* **2011,** 158, (4), 774-789.
40. Mathieu, O.; Levacque, A.; Petersen, E. L., Effects of N2O addition on the ignition of H-2-O-2 mixtures: Experimental and detailed kinetic modeling study. *Int. J. Hydrogen Energy* **2012,** 37, (20), 15393-15405.
41. Mathieu, O.; Levacque, A.; Petersen, E. L., Effects of NO2 addition on hydrogen ignition behind reflected shock waves. *Proc. Combust. Inst.* **2013,** 34, 633-640.
42. Mulvihill, C. R.; Mathieu, O.; Petersen, E. L., The unimportance of the reaction H2 + N2O reversible arrow H2O + N2: A shock-tube study using H2O time histories and ignition delay times. *Combust. Flame* **2018,** 196, 478-486.
43. Kobayashi, H.; Hayakawa, A.; Somarathne, K. D. Kunkuma A.; Okafor, Ekenechukwu C., Science and technology of ammonia combustion. *Proc. Combust. Inst.* **2019,** 37, (1), 109-133.
44. Tsang, W.; Herron, J. T., Chemical Kinetic Data-Base for Propellant Combustion .1. Reactions Involving NO, NO2, HNO, HNO2, HCN and N2O. *J. Phys. Chem. Ref. Data* **1991,** 20, (4), 609-663.
45. Fulle, D.; Hamann, H. F.; Hippler, H.; Troe, J., Temperature and pressure dependence of the addition reactions of HO to NO and to NO2. IV. Saturated laser-induced fluorescence measurements up to 1400 bar. *J. Chem. Phys.* **1998,** 108, (13), 5391-5397.
46. Atkinson, R.; Baulch, D. L.; Cox, R. A.; Crowley, J. N.; Hampson, R. F.; Hynes, R. G.; Jenkin, M. E.; Rossi, M. J.; Troe, J., Evaluated kinetic and photochemical data for atmospheric chemistry: Volume I - gas phase reactions of O-x, HOx, NOx and SOx species. *Atmos. Chem. Phys.* **2004,** 4, 1461-1738.
47. Ko, T.; Fontijn, A., High-Temperature Photochemistry Kinetics Study of the Reaction H + NO2 -> OH + NO from 296 K to 760 K. *J. Phys. Chem.* **1991,** 95, (10), 3984-3987.
48. Su, M. C.; Kumaran, S. S.; Lim, K. P.; Michael, J. V.; Wagner, A. F.; Harding, L. B.; Fang, D. C., Rate constants,

1100 <= T <= 2000 K, for H+NO2 -> OH+NO using two shock tube techniques: Comparison of theory to experiment. *J. Phys. Chem. A* **2002,** 106, (36), 8261-8270.

49. Haas, F. M.; Dryer, F. L., Rate Coefficient Determinations for H + NO2 -> OH plus NO from High Pressure Flow Reactor Measurements. *J. Phys. Chem. A* **2015,** 119, (28), 7792-7801.

50. Burkholder, J. B.; Mellouki, A.; Talukdar, R.; Ravishankara, A. R., Rate Coefficients for the Reaction of OH with HONO between 298-K and 373-K. *Int. J. Chem. Kinet.* **1992,** 24, (8), 711-725.

51. Xia, W. S.; Lin, M. C., Ab initio MO/statistical theory prediction of the OH plus HONO reaction rate: evidence for the negative temperature dependence. *Physchemcomm* **2000,** 3, 71-78.

52. Shang, Y.; Shi, J.; Ning, H.; Zhang, R.; Wang, H.; Luo, S., Ignition delay time measurements and kinetic modeling of CH4 initiated by CH3NO2. *Fuel* **2019,** 243, 288-297.

53. Song, Y.; Hashemi, H.; Christensen, J. M.; Zou, C.; Marshall, P.; Glarborg, P., Ammonia oxidation at high pressure and intermediate temperatures. *Fuel* **2016,** 181, 358-365.

54. Grimme, S.; Ehrlich, S.; Goerigk, L., Effect of the Damping Function in Dispersion Corrected Density Functional Theory. *J. Comput. Chem.* **2011,** 32, (7), 1456-1465.

55. Klippenstein, S. J., From theoretical reaction dynamics to chemical modeling of combustion. *Proc. Combust. Inst.* **2017,** 36, (1), 77-111.

56. Wang, Q.-D.; Sun, M.-M.; Liang, J.-H., Reaction Mechanisms and Kinetics of the Hydrogen Abstraction Reactions of C4–C6 Alkenes with Hydroxyl Radical: A Theoretical Exploration. *Int. J. Mol. Sci.* **2019,** 20, (6), 1275.

57. Goldsmith, C. F.; Green, W. H.; Klippenstein, S. J., Role of O-2 + QOOH in Low-Temperature Ignition of Propane. 1. Temperature and Pressure Dependent Rate Coefficients. *J. Phys. Chem. A* **2012,** 116, (13), 3325-3346.

58. Lee, T. J.; Taylor, P. R., A Diagnostic for Determining the Quality of Single-Reference Electron Correlation Methods. *Int. J. Quantum Chem* **1989**, 199-207.

59. Goldsmith, C. F.; Magoon, G. R.; Green, W. H., Database of Small Molecule Thermochemistry for Combustion. *J. Phys. Chem. A* **2012,** 116, (36), 9033-9057.

60. Johnston, H. S.; Heicklen, J., Tunnelling Corrections for Unsymmetrical Eckart Potential Energy Barriers. *J. Phys. Chem.* **1962,** 66, (3), 532-533.

61. Barker, J. R., Multiple-well, multiple-path unimolecular reaction systems. I. MultiWell computer program suite. *Int. J. Chem. Kinet.* **2001,** 33, (4), 232-245.

62. Nguyen, T. L.; Stanton, J. F., High-level theoretical study of the reaction between hydroxyl and ammonia: Accurate rate constants from 200 to 2500 K. *J. Chem. Phys.* **2017,** 147, (15), 152704.

63. Nguyen, T. L.; Stanton, J. F., Ab initio thermal rate coefficients for H + NH3 = H2 + NH2. *Int. J. Chem. Kinet.* **2019,** 51, (5), 321-328.

64. Michael, J. V.; Sutherland, J. W.; Klemm, R. B., Rate-Constant for the Reaction H + NH3 over the Temperature-Range 750-1777 K. *J. Phys. Chem.* **1986,** 90, (3), 497-500.

65. Nilsson, E. J. K.; Konnov, A. A., Role of HOCO Chemistry in Syngas Combustion. *Energy Fuels* **2016,** 30, (3), 2443-2457.

66. Mathieu, O.; Petersen, E. L., Experimental and modeling study on the high-temperature oxidation of Ammonia and related NOx chemistry. *Combust. Flame* **2015,** 162, (3), 554-570.

67. Abian, M.; Alzueta, M. U.; Glarborg, P., Formation of NO from N2/O2Mixtures in a Flow Reactor: Toward an Accurate Prediction of Thermal NO. *Int. J. Chem. Kinet.* **2015,** 47, (8), 518-532.

68. Dayma, G.; Dagaut, P., Effects of Air Contamination on the Combustion of Hydrogen—Effect of NO and NO2 Addition on Hydrogen Ignition and Oxidation Kinetics. *Combust. Sci. Technol.* **2006,** 178, (10-11), 1999-2024.

69. Mevel, R.; Lafosse, F.; Chaumeix, N.; Dupre, G.; Paillard, C. E., Spherical expanding flames in H-2-N2O-Ar mixtures: flame speed measurements and kinetic modeling. *Int. J. Hydrogen Energy* **2009,** 34, (21), 9007-9018.